α_{1C}-subunit (RGAPAGLHDQKKG+C). A male Japanese White rabbit was immunized four times every 2 wk. Serum was collected, and polyclonal antibody was affinity purified.

Immunoblotting. The membrane fraction was prepared and immunoblotting was performed as described previously (23). Briefly, tissues from rat (DA, aorta, atria, left ventricle, and lung) were homogenized in an ice-cold buffer [in mM: 50 Tris (pH 8.0), 1 EDTA, 1 EGTA, 1 dithiothreitol, and 200 sucrose] and protease inhibitors (Complete Mini, Roche, Tokyo, Japan). The polyclonal antibody specific for α_{1C}-, α_{1D}-, and α_{1G}-subunits (Chemicon, Temecula, CA) or spliced variant of α_{1C}-subunit at 5 μg/ml was used to examine 20-μg membrane fractions from rat tissues.

Immunohistochemistry. For immunoperoxidase demonstration of VDCCs in the DA, paraffin-embedded blocks containing DA tissues were cut into 4-μm-thick sections and placed on 3-aminopropyltriethoxysilane-coated glass slides. To determine the boundary line of intimal cushion formation, tissue sections were stained with Elastica van Gieson as recommended by the manufacturer (Muto Pure Chemicals). The specimens were deparaffinized, rehydrated, and incubated for 5 min in peroxidase-blocking reagent (DAKO Laboratories) to inactivate endogenous peroxidases. Slides were incubated with each primary antibody of splicing variant of α_{1C}-, α_{1D}-, α_{1G}-, and α_{1C}-subunits (1:200 dilution) at room temperature for 30 min. After they were washed with 0.1 M PBS for 5 min, the slides were incubated for 30 min in biotinylated rabbit anti-goat IgG (Vector, Burlingame, CA). Then the slides were washed with 0.1 M PBS for 5 min, incubated for 30 min in avidin-biotin-horseradish peroxidase complex (Vector), and washed again with 0.1 M PBS for 5 min. The peroxidase reactivity was demonstrated with 3,3'-diaminobenzidine (Sigma, St. Louis, MO) and 0.3% H_2O_2 for 5 min. The specificity of staining was examined by omission of the primary antibodies. The slides were counterstained with Mayer's hematoxylin.

Primary culture of rat DA SMCs. Vascular SMCs in primary culture were obtained from the DA of Wistar rat embryos at e21. The tissues were minced and transferred to a 1.5-ml centrifuge tube that contained 800 μl of collagenase-dispase enzyme mixture [1.5 mg/ml collagenase-dispase (Roche), 0.5 mg/ml elastase type II-A (Sigma Immunochemicals, St. Louis, MO), 1 mg/ml trypsin inhibitor type I-S (Sigma), and 2 mg/ml bovine serum albumin fraction V (Sigma) in Hanks' balanced salt solution (Sigma)]. The digestion was carried out at 37°C for 15–20 min. Then cell suspensions were centrifuged, and the medium was changed to the collagenase II enzyme mixture [1 mg/ml collagenase II (Worthington), 0.3 mg/ml trypsin inhibitor type I-S, and 2 mg/ml bovine serum albumin fraction V in Hanks' balanced salt solution]. After 12 min of incubation at 37°C, cell suspensions were transferred to growth medium in 35-mm poly-L-lysine (Sigma)-

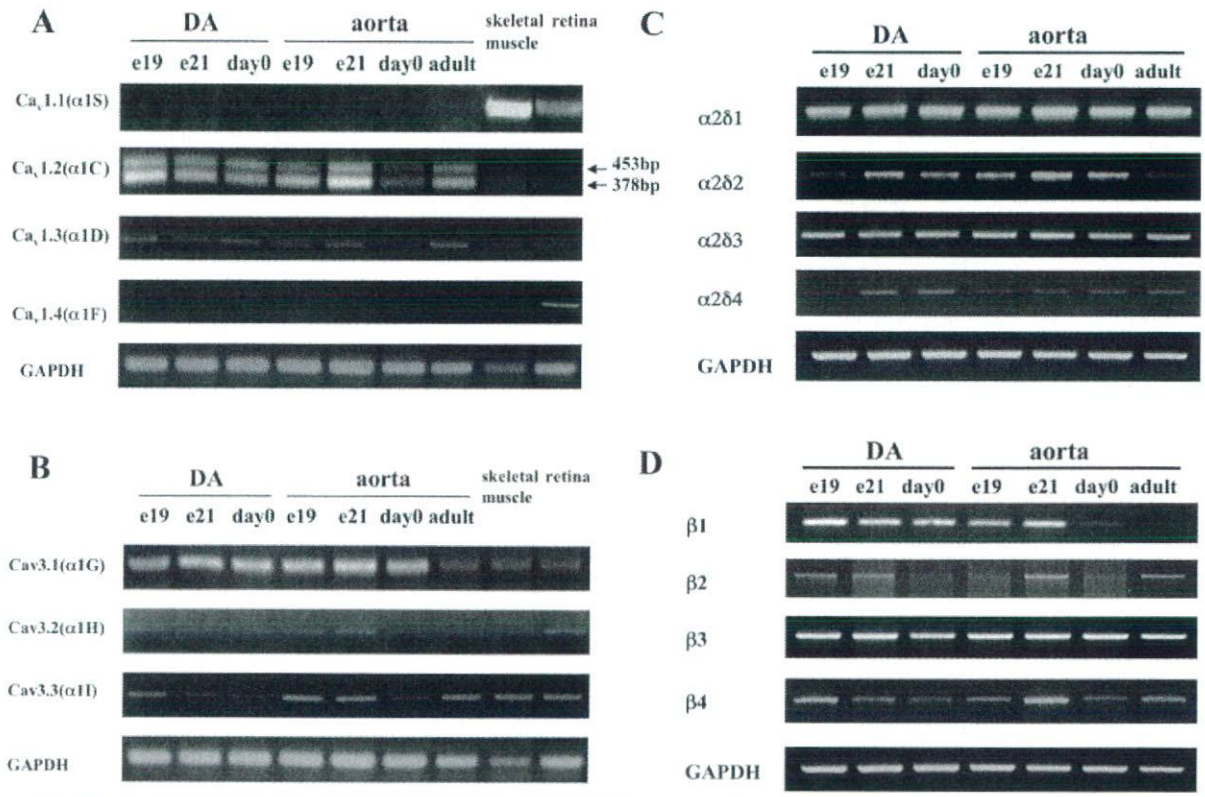

Fig. 1. Semiquantitative RT-PCR analyses of Ca^{2+} channel subunits. *A*: RT-PCR for L-type Ca^{2+} channel α_1-subunit isoforms in rat ductus arteriosus (DA), aorta, skeletal muscle, and retina. RNA samples from tissues were processed for 35 cycles of PCR using primers directed to the cDNA sequence of VDCC α_{1S}-, α_{1C}-, α_{1D}-, and α_{1F}-isoforms. PCR of the primer alone, without template, resulted in no product (data not shown). Transcripts for α_{1C}- and α_{1D}-subunits were detected in DA and aorta, but no transcripts for α_{1S}- and α_{1F}-subunits were detected in DA and aorta. Transcripts for α_{1C}-subunit were detected as clear bands of expected (378 bp) and longer (453 bp) lengths. Sequence analysis detected insertion of an unreported 75-bp cDNA in the 453-bp band into the 378-bp band. Expression of α_{1C}-subunit mRNA was not altered during development. Expression of α_{1D}-subunit mRNA was decreased in DA from embryonic *day 21* (e21) but decreased from *day 0* (birth) in aorta. *B*: RT-PCR for T-type Ca^{2+} channel α_{1G}-, α_{1H}-, and α_{1I}-subunits in rat DA, aorta, skeletal muscle, and retina. Transcripts for these subunits were present in DA and aorta. Expression level of α_{1G}-subunit mRNA was high from embryonic *day 19* (e19) to *day 0* in DA and aorta and decreased in adult aorta. Levels of α_{1H}- and α_{1I}-subunit mRNA expression were low in DA and aorta. *C*: RT-PCR for $\alpha_{2\delta}$-subunits in rat DA and aorta during development. Transcripts for all 4 $\alpha_{2\delta}$-subunit isoforms were present in both tissues. *D*: RT-PCR for β-subunits in rat DA and aorta during development. Transcripts for 4 β-isoforms were present in both tissues. β_3-Subunit mRNA was abundant in DA and aorta throughout development.

coated dishes in a moist tissue culture incubator at 37°C in 5% CO_2-95% ambient mixed air. The growth medium contained DMEM with 10% FCS, 100 U/ml penicillin, and 100 mg/ml streptomycin (Invitrogen). The confluent cells were used at *passages 4–6*. We confirmed that >99% of cells were positive for α-smooth muscle actin and showed the typical "hill-and-valley" morphology.

Cell proliferation assays. [^{3}H]thymidine incorporation was used to measure cell proliferation in DA SMCs. The SMCs were reseeded into a 24-well culture plate at an initial density of 1×10^5 cells per well for 24 h before serum starvation with DMEM containing 0.5% FCS. Cells were then incubated with or without nitrendipine (1 μM), kurtoxin (1 μM), and efonidipine (3 μM) for 16 h in the starvation medium before addition of 1 μCi of [*methyl*-^{3}H]thymidine (specific activity 5 Ci/mM; Amersham International, Bucks, UK) for 4 h at 37°C. After fixation with 1.0 ml of 10% trichloroacetic acid, the cells were solubilized with 0.5 ml of 0.5 M NaOH and then neutralized with 0.25 ml of 1 N HCl. A liquid scintillation counter was used to measure [^{3}H]thymidine incorporation. Data obtained from triplicate wells were averaged.

Generation of expression construct for spliced variant of rat α_{1C}-subunit. The 220-bp fragment containing a 75-bp insertion of the spliced variant of rat VDCC α_{1C}-subunit was extracted from the 453-bp PCR fragment using *Xho* I and *Sph* I restriction enzymes. Then the 220-bp fragment was introduced into the *Xho I*/*Sph* I site of the pcDNA3.1(+)-based expression construct of the rat brain 1C subunit (rbCII; kindly supplied by Dr. T. P. Snutch) (35). The sequence of the expression construct was confirmed by direct sequencing analysis.

Electrophysiological recordings. $Ca_V1.2$ (rbCII; GenBank accession no. M67515) or its mutant was transiently expressed in BHK6 cells, which stably express β_1- and $\alpha_{2\delta}$-subunits. Transfection was carried out with a transfection reagent (FuGene 6, Roche), as previously described (43).

Electrophysiological recordings were performed in the whole cell patch-clamp configuration using a patch/whole cell-clamp amplifier (Axopatch 200B, Axon Instruments) and an analog-to-digital converter (Digidata 1200, Axon Instruments) (43). Data acquisition was performed with pCLAMP7 software (Axon Instruments). Signals were filtered at 5 kHz. Capacitative currents were electrically compensated. The P/4 protocol (pCLAMP7) was used for leak subtraction. Ca^{2+} currents and Ba^{2+} currents (I_{Ba}) through $Ca_V1.2$ (rbCII) Ca^{2+} channels expressed in BHK6 cells were measured as previously described (27). The external solution contained (in mM) 137 NaCl, 5.4 KCl, 1 $MgCl_2$, 10 HEPES, and 10 glucose, with 2 $CaCl_2$ or $BaCl_2$ as a charge carrier; pH was adjusted to 7.4 with NaOH at room temperature. The resistance of the patch electrode was 2–2.5 MΩ when it was filled with the pipette solution containing (in mM) 120 $CsMeSO_4$, 20 TEA-Cl, 14 EGTA, 5 Mg-ATP, 5 Na_2 creatine phosphate, 0.2 GTP, and 10 HEPES, with pH adjusted to 7.3 with CsOH at room temperature. All experiments were carried out at room temperature.

The half-activation potential ($V_{h\text{-}act}$) was estimated by fitting the current-voltage (*I-V*) relations (curves) to the following equation by an interactive nonlinear regression fitting procedure

$$I = (V_m - V_{rev}) * G_{max} * \{1/[1 + \exp(V_m - V_{h\text{-}act})/k]\}$$

where V_m is membrane potential, V_{rev} is reversal potential, k is slope factor, and G_{max} is maximum conductance.

Half-inactivation voltage ($V_{h\text{-}inact}$) was estimated by fitting the steady-state inactivation curves to the following equation

$$I = I_{min} + (I_{max} - I_{min})/[1 + \exp(V_{h\text{-}inact} - V)/k]$$

where I_{max} and I_{min} are maximum and minimum plateau currents, respectively, and k is slope factor.

Statistical analysis. Values are means ± SE. Student's unpaired *t*-tests and unpaired ANOVA followed by the Student-Newman-Keuls test were used for statistical analysis. $P < 0.05$ was considered statistically significant.

RESULTS

Multiple transcripts of VDCC α_1-, $\alpha_{2\delta}$-, and β-subunits in rat DA. Semiquantitative RT-PCR analyses revealed that, among voltage-dependent L-type Ca^{2+} channel subunits, α_{1C}- and α_{1D}-subunit mRNAs were expressed in the DA and the aorta, whereas neither α_{1F}- nor α_{1S}-subunit transcript was detected (Fig. 1*A*). The α_{1C}-subunit transcripts were amplified as two bands, 378 bp (the expected size) and 453 bp, in the RT-PCR products. The 378-bp band was confirmed as the reported VDCC α_{1C}-subunit, and the 453-bp band was identified as a novel spliced variant of the rat VDCC α_{1C}-subunit by sequencing analysis. Another spliced variant of α_{1C}-subunit in the human, which displayed oxygen-sensitive opening of the channel, was recently identified (11). However, we could not detect this spliced variant in DA, aorta, and genomic DNA in the rat by RT-PCR using $Ca_V1.2$ (α_{1C})-2 primers, although we could detect its expression in human right ventricle (data not shown). The expression of VDCC α_{1A} (P/Q-type)-, α_{1B} (N-type)-, and α_{1E} (R-type)-subunits was not detected in the DA by semiquantitative RT-PCR (data not shown).

The transcripts of all T-type Ca^{2+} channel α_1-subunits, α_{1G}, α_{1H}, and α_{1I}, were detected in the DA and aorta (Fig. 1*B*). In our PCR conditions, expression of the α_{1G}-isoform was highest and expression of the α_{1H}-isoform was lowest in the DA among T-type Ca^{2+} channel α_1-subunits. Expression of α_{1I} was decreased from e21 in the DA and from *day 0* in the aorta.

The transcripts of all four $\alpha_{2\delta}$-subunits were detected in the DA and aorta (Fig. 1*C*). Transcripts of all four β-subunits were detected in the DA and aorta (Fig. 1*D*). Among them, β_3-subunit mRNA was highly expressed by semiquantitative RT-PCR during development in the DA and aorta. Expression of β_3-subunit mRNA was not changed during development. Expression of β_1-subunit mRNA was not detected in adult aorta.

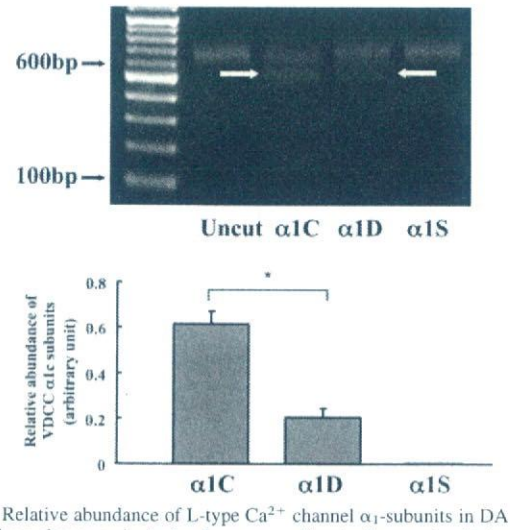

Fig. 2. Relative abundance of L-type Ca^{2+} channel α_1-subunits in DA at e21. Uncut lane shows a single band corresponding to fragments obtained after RT-PCR; α_{1C}, α_{1D}, and α_{1S} lanes show fragments obtained after restriction digest with enzymes. Digested fragments are indicated by arrows. Digested fragment was detected more in α_{1C}- than in α_{1D}-subunit. No digested fragment was detected in α_{1S}-subunit. Values for α_{1C}- and α_{1D}-subunits were obtained from the value into which elements digested by each enzyme were divided by amount of uncut PCR product using densitometry. The α_{1C}-subunit is the most abundant of the L-type Ca^{2+} channel subunits. *$P < 0.01$.

Expression β_2- and β_4-subunit mRNA was higher in the fetus than that in neonates on *day 0*.

VDCC α_{1C}-subunit was a predominant transcript of L-type Ca^{2+} channel subunits in rat DA. Using restriction enzyme analysis as previously reported (29), we determined relative abundance of HVA Ca^{2+} channel mRNA. The digested fragments were detected only in the α_{1C}- and α_{1D}-subunit lanes (Fig. 2), which is consistent with the result from semiquantitative RT-PCR. The values of α_{1C}- and α_{1D}-subunits were obtained when the value into which elements digested by each enzyme was divided by the amount of uncut PCR product. The density of the digested fragment was significantly higher in the α_{1C}- than in the α_{1D}-subunit lane, indicating that the α_{1C}-subunit is the most abundant transcript among L-type Ca^{2+} channel subunits.

Protein expression of α_{1C}-, α_{1D}-, α_{1G}-, and β_3-subunits in the DA. Protein expression of α_{1C}-, α_{1D}-, α_{1G}-, and β_3-subunits was examined by immunoblotting analysis (Fig. 3). Although the expression level of α_{1C}-subunit mRNA was higher in the DA than in the fetal aorta, the expression level of α_{1C}-subunit protein in the DA was comparable with that in the aorta at e21 and much less than that in the adult atrium and aorta. Protein expression of the α_{1D}-subunit was similarly detected in the DA and aorta at e21, but not in the adult aorta. The level of α_{1G}-subunit protein expression was high in the DA and aorta at e21 and undetectable in the adult aorta. We also detected β_3-subunit protein expression in the DA at e21.

In addition, we examined the localization of α_{1C}-, α_{1D}-, and α_{1G}-subunit proteins in the DA at e21 by immunostaining with anti-α_{1C}, -α_{1D}, and -α_{1G} (Fig. 3*B*). Strong immunoreaction of α_{1C}- and α_{1G}-subunits and moderate immunoreaction of the α_{1D}-subunit were found in SMCs in the DA. Especially, the α_{1G}-subunit was strongly expressed in the region of intimal thickening of the DA, which is clearly distinguished by Elastica stain.

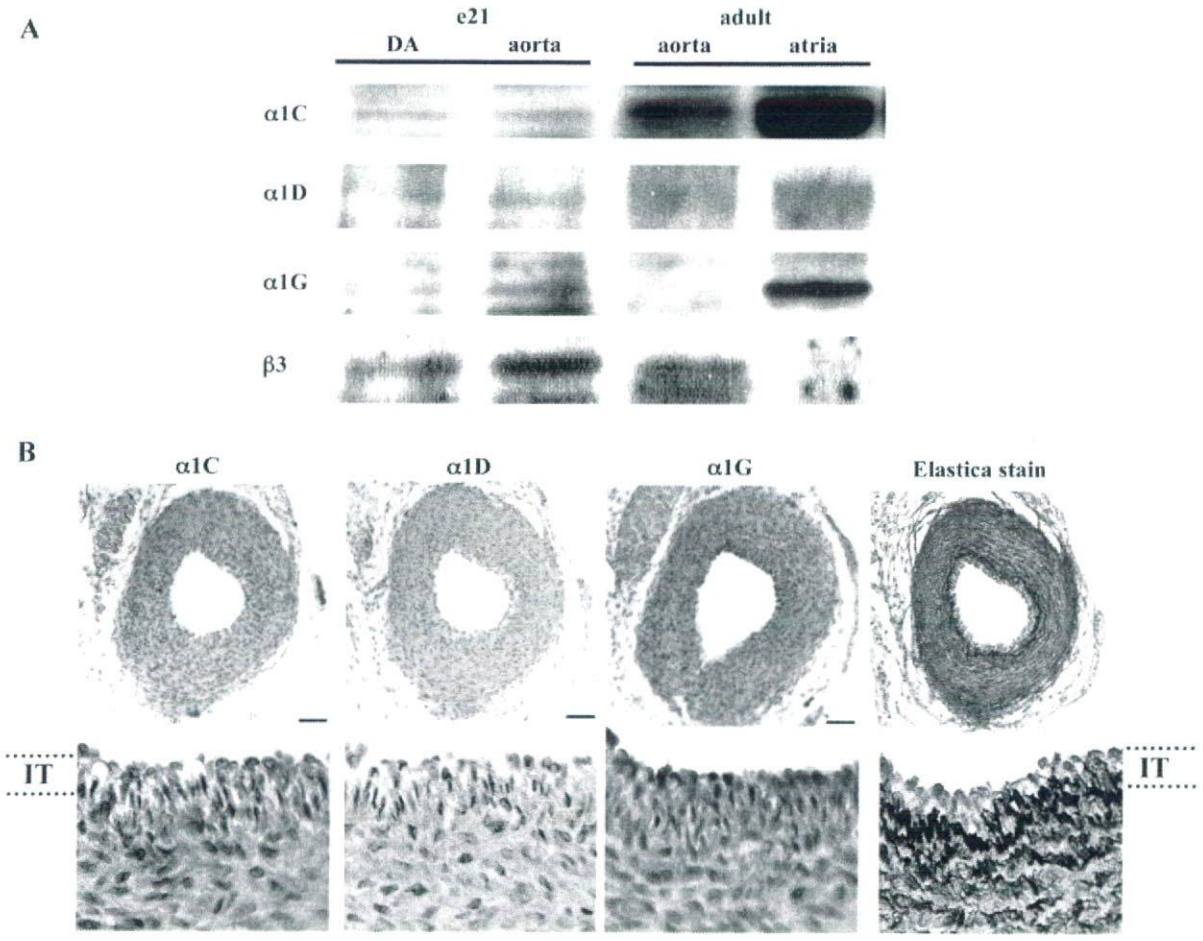

Fig. 3. *A*: expression of α_{1C}-, α_{1D}-, α_{1G}-, and β_3-subunit protein in rat DA, aorta, and atrium by immunoblotting. Membrane proteins from rat tissues were separated by SDS-PAGE, together with prestained molecular weight markers, and subjected to immunoblot analysis with each subunit-selective antibody. Expression level of α_{1C}-subunit protein was comparable in DA and aorta at e21 and much less in DA than in adult atrium. Expression of α_{1D}-subunit was similarly detected in DA and aorta at e21. Expression of α_{1G}-subunit protein was high in DA and aorta at e21 and undetectable in adult aorta. Expression of β_3-subunit was high in DA at e21. *B*: DA at e21 immunostained with anti-α_{1C}, -α_{1D}, and -α_{1G}. Elastica stain identified the boundary of intimal cushion formation. High-magnification (×4) image of the region of intimal cushion formation is shown at *bottom*. Strong immunoreaction of α_{1C}-subunit and mild immunoreaction of α_{1D}-subunit were ubiquitously found in DA. Strong α_{1G}-subunit immunoreaction was especially found at the region of intimal thickening (IT) in DA. Scale bar, 100 μm.

Effects of development and maternally administered vitamin A on expression of VDCC α_1-subunit transcripts. Although the expression levels of α_{1C}-subunit mRNA were not changed in the DA during development, a significant decrease in the expression level of α_{1C}-subunit mRNA in the aorta resulted in a higher expression of α_{1C}-subunit mRNA in the DA than in the aorta after e21 (Fig. 4*A*). Maternally administered vitamin A significantly increased the expression levels of α_{1C}-subunit mRNA at *day 0* ($P < 0.01$; Fig. 4*B*).

Expression of α_{1G}-subunit mRNA was 25–120 times higher in perinatal vessels than in the adult aorta (Fig. 4*C*). The expression was upregulated in the DA during development. The level of α_{1G}-subunit mRNA was significantly higher in the DA than in the aorta at *day 0*. Maternally administered vitamin A significantly upregulated the expression of α_{1G}-subunit mRNA at all developmental stages ($P < 0.001$; Fig. 4*D*).

Effects of L- and T-type VDCCs on SMC proliferation in DA. We used a specific L-type VDCC blocker (nitrendipine), a specific T-type VDCC blocker (kurtoxin), and an L- and T-type VDCC blocker (efonidipine) to investigate a role for VDCCs in SMC proliferation in the DA. Significant inhibition of [^{3}H]thymidine incorporation was observed in rat DA SMCs treated with 1 μM nitrendipine, 3 μM efonidipine, or 1 μM kurtoxin compared with untreated SMCs (Fig. 5). The inhibition was the strongest in SMCs treated with 3 μM efonidipine, suggesting that the additive inhibitory effect of efonidipine on cell proliferation is due to the blockade of L- and T-type VDCCs in rat DA SMCs.

A novel spliced variant of the α_{1C}-subunit was highly expressed in adult lung and fetal arteries. As demonstrated above, using RT-PCR with $Ca_v1.2$ (α_{1C})-1 primers, we found a novel alternatively spliced isoform of the α_{1C}-subunit in the DA and aorta (Table 1). The PCR products were subcloned into a pCRII vector (Invitrogen) and sequenced. We reported the nucleotide sequence in the EMBL/GenBank nucleotide sequence databases (accession no. AY323810; Fig. 6*A*). The spliced variant contained a 26-amino acid insertion into the I-II cytoplasmic linker that interacts with the β-subunit of α_{1C} (Fig. 6*B*). During the course of the present study, homologs of this variant have been reported in other species. Figure 6*C* shows

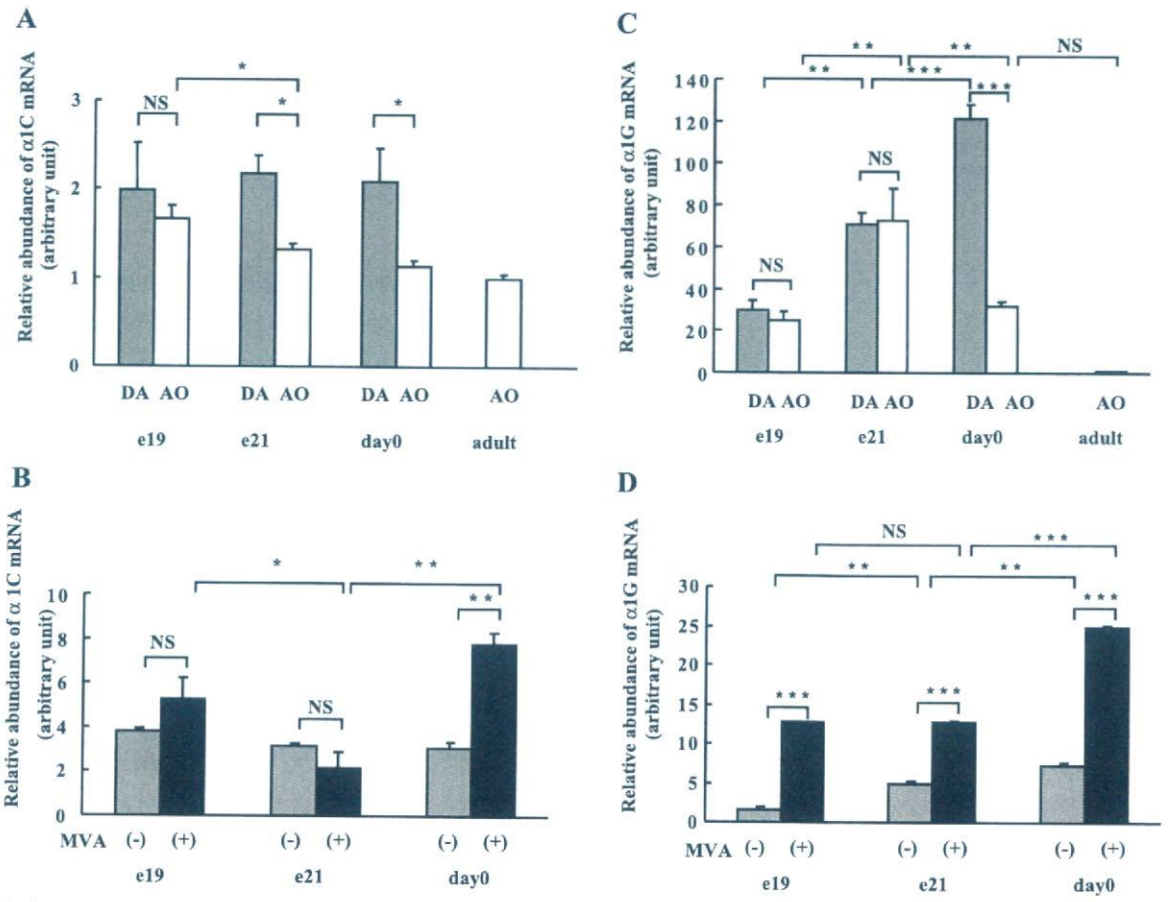

Fig. 4. *A*: developmental changes in expression of α_{1C}-subunit mRNA. Expression level of α_{1C}-subunit mRNA was higher in DA than in aorta (AO) at e21 and *day 0*. Expression level was not changed in DA during development but was decreased in aorta from e19 to e21. $^*P < 0.05$. NS, not significant. *B*: effects of maternally administered vitamin A (MVA) on expression of α_{1C}-subunit mRNA in DA. Levels of α_{1C}-subunit mRNA were not changed in DA during development and were significantly increased with vitamin A only at *day 0*. $^*P < 0.05$; $^{**}P < 0.01$. *C*: developmental changes in expression of α_{1G}-subunit mRNA. Transcripts for α_{1G}-subunit were increased during development in DA. Abundance of α_{1G}-subunit mRNA was significantly greater in DA than in aorta at *day 0*. $^{**}P < 0.01$; $^{***}P < 0.001$. *D*: effects of maternally administered vitamin A on expression of α_{1G}-subunit mRNA in DA. Expression of α_{1G}-subunit mRNA was upregulated during development and significantly higher than with vitamin A at any developmental stage. $^{**}P < 0.01$; $^{***}P < 0.001$.

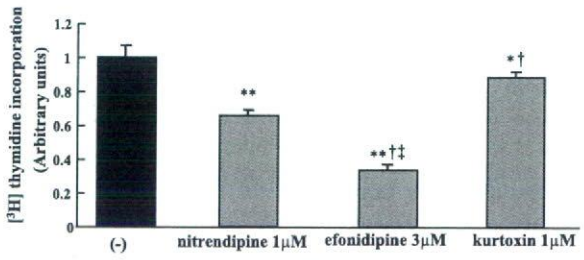

Fig. 5. Effects of VDCC blockers on [^{3}H]thymidine uptake of DA smooth muscle cells. [^{3}H]thymidine incorporation in groups treated with nitrendipine, efonidipine, and kurtoxin was decreased compared with that in control group in 0.1% FCS-containing medium. Treatment of DA smooth muscle cells with efonidipine resulted in additional reduction of [^{3}H]thymidine uptake compared with nitrendipine or kurtoxin treatment. Experiments were performed 3 times independently in duplicate. Significantly different from control: $*P < 0.01$, $**P < 0.0001$. †Significantly different from nitrendipine ($P < 0.01$). ‡Significantly different from kurtoxin ($P < 0.01$).

that amino acid sequence homology between the rat and other species (mouse, rabbit, and human) is very high (100%, 92%, and 88%, respectively).

We characterized the novel spliced isoform of rat α_{1C}-subunit. Figure 7*A* shows the expression the spliced variant of α_{1C}-subunit mRNA and protein by semiquantitative RT-PCR and immunoblotting analyses. The PCR product migrating 453 bp was the spliced variant of the α_{1C}-subunit and the 378-bp band indicated the reported α_{1C}-subunit. A relatively high intensity of the 453-bp band was detected in the DA and the aorta. Using the specific antibody against the spliced variant of the α_{1C}-subunit, we also found a high level of expression of the variant protein in arteries, including the DA, and less expression in the adult heart.

By quantitative RT-PCR analyses, the spliced variant transcript was expressed most abundantly in the adult lung (data not shown), less in the fetal arteries, and least in the adult arteries. In other adult tissues, the expression level of α_{1C}-subunit mRNA, including this spliced variant, was very low (data not shown). The ratio of the abundance of the spliced variant to the conventional α_{1C}-isoform was measured by quantitative RT-PCR (see MATERIALS AND METHODS). The proportion of the spliced variant and nonspliced α_{1C}-isoform was almost invariable (1–1.5) among the lung, DA, and aorta. Furthermore, we examined the developmental changes in the expression of the spliced variant of the α_{1C}-subunit transcript in the DA and aorta (Fig. 7*B*). The level of the spliced variant α_{1C}-subunit mRNA peaked at e21 in the DA. After birth, the level of the spliced variant α_{1C}-subunit mRNA was higher in the DA than in the aorta.

Localization of the spliced variant of the α_{1C}-subunit in the DA at e21 was examined by immunostaining with anti-α_{1C}-subunit splicing variant (Fig. 7*C*). Strong immunoreaction was found in the region of intimal thickening of the DA (Fig. 7*C*, *right*), whereas immunoreaction of the conventional α_{1C}-isoform was ubiquitously expressed in the whole layers of the DA (Fig. 3*B*).

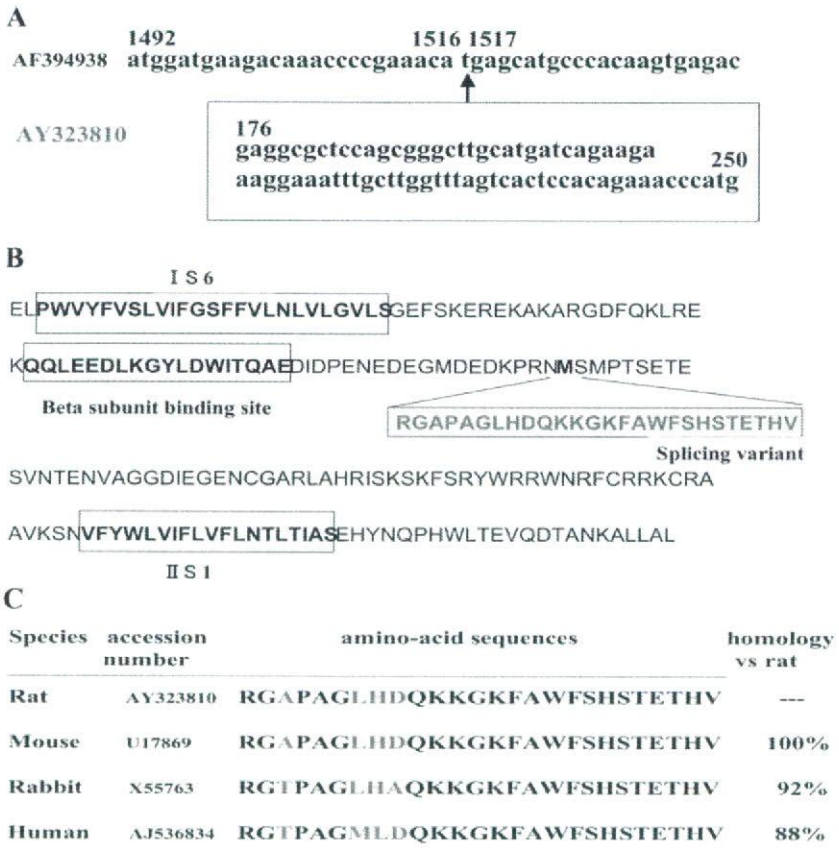

Fig. 6. *A*: alignment of nucleotide sequence of rat Ca^{2+} channel α_{1C}-subunit (GenBank accession no. AF394938) and novel spliced variant (GenBank accession no. AY323810). Spliced variant consists of a 75-bp insertion. *B*: amino acid sequence of rat Ca^{2+} channel α_{1C}-subunit. Spliced variant contains a 25-amino acid insertion into the I-II cytoplasmic linker that interacts with the β-subunit of α_{1C}. *C*: comparison of amino acid sequence of novel α_{1C}-subunit alternatively spliced isoform among several species. Sets of conservative or unconservative residues are indicated in bold or light font, respectively. Amino acid sequence is highly conserved among species.

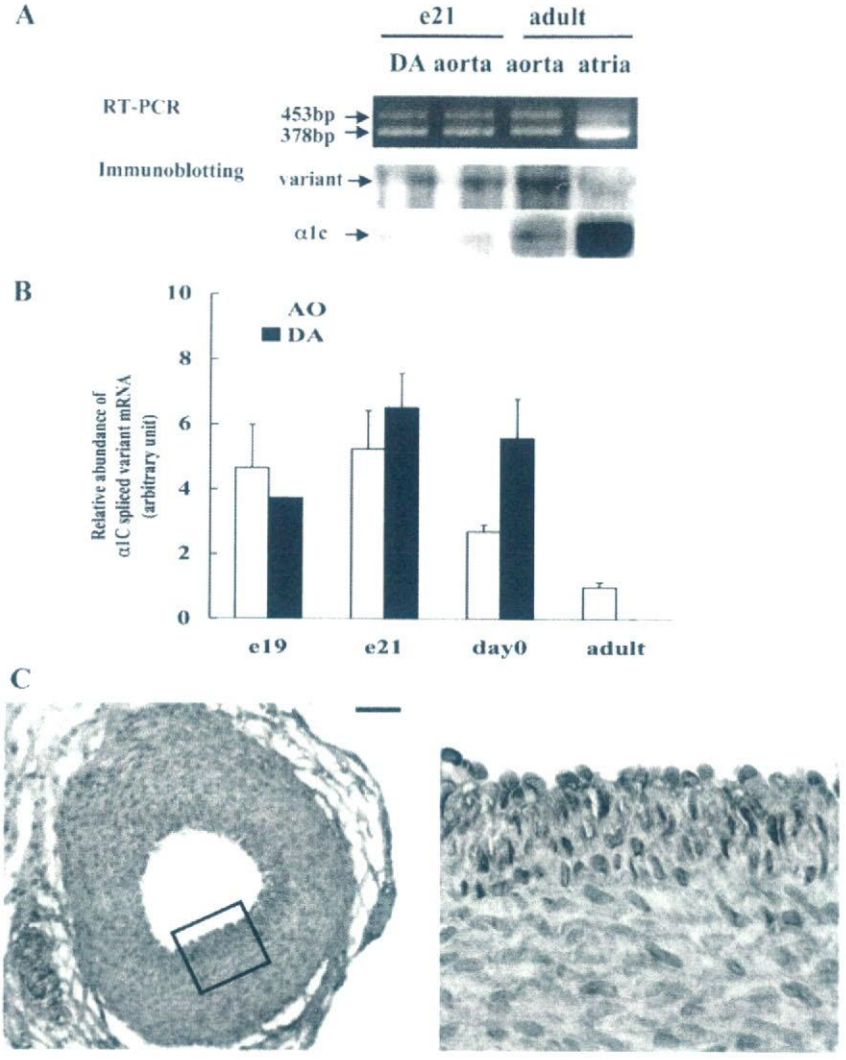

Fig. 7. *A*: expression of splicing variant of α_{1C}-subunit confirmed by semiquantitative RT-PCR and immunoblotting analyses. Band migrating at 453 bp is spliced variant of α_{1C}-subunit; smaller band is nonspliced α_{1C}-isoform. Immunoblotting analysis revealed that spliced variant of α_{1C}-subunit was highly expressed in vascular smooth muscle, including DA, at mRNA and protein levels. *B*: relative abundance of spliced variant of α_{1C}-subunit mRNA measured by quantitative RT-PCR. Level of spliced variant of α_{1C}-subunit mRNA is highly expressed in DA and aorta in the fetus. *C*: immunoreaction of splicing variant of α_{1C}-subunit was found in smooth muscle cells of DA at e21. Strong immunoreaction was found in region of intimal thickening. Scale bar, 100 μm. High-magnification (×4) image of region enclosed in rectangle at *left* is shown at *right*.

We examined whether the DA variant exerts any differences in the gating kinetics of the Ca^{2+} channel. Activation and inactivation kinetics of I_{Ba} were not significantly different between rbCII and the DA variant (Fig. 8*A*). The expression level at the surface membrane, estimated as the density of I_{Ba}, did not differ between the two groups, even though the individual cell showed a wide variety of I_{Ba} density, as is often the case with a transient expression experiment (Fig. 8*B*). The *I-V* relations of rbCII and the DA variant were almost superimposable (Fig. 8*C*). $V_{h\text{-}act}$ of rbCII and the DA variant were -15.4 ± 1.9 mV ($n = 9$) and -14.5 ± 1.2 mV ($n = 7$), respectively (not statistically significant). The steady-state inactivation curves could be slightly shifted toward the depolarized direction in the DA variant, but $V_{h\text{-}inact}$ was not significantly different: -33.3 ± 1.0 mV ($n = 9$) and -31.5 ± 1.7 mV ($n = 6$), respectively.

DISCUSSION

Ca^{2+} influx through VDCCs plays an important role in vascular myogenic reactivity and tone (4, 8, 26). To our knowledge, the present study demonstrated the first complete characterization of the expression of VDCC subtype mRNAs in the DA. Tristani-Firouzi et al. (38) demonstrated that activation of L-type, but not T-type, VDCCs plays a major role in oxygen-sensitive contraction in the DA. Takizawa et al. (37) demonstrated that an L-type VDCC blocker, verapamil, inhibits spontaneous closure of the DA in newborn rats. Therefore, the abundant expression of α_{1C}-subunit mRNA in the DA suggested that the α_{1C}-subunit is mainly responsible for the influx of Ca^{2+} that induces contraction of the DA after birth.

We also found that all T-type VDCCs were expressed in the DA. The most dominant isoform among T-type VDCCs in the DA is the α_{1G}-subunit, with an expression level 25–120 times higher in fetal vessels than in adult aorta, which is consistent with previous reports showing that T-type VDCCs are predominantly expressed in the early stages of differentiation of many embryonic and neonatal tissues (2, 9, 12, 21). The expression of α_{1G}-subunit mRNA was significantly upregulated by maternal administration of vitamin A. In the DA, α_{1G}-subunit protein was highly localized in the region of intimal thicken-

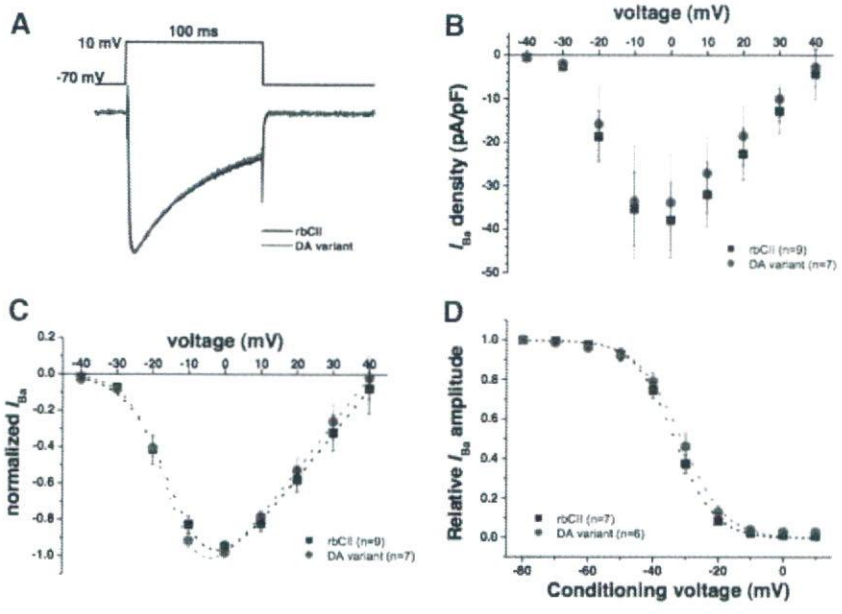

Fig. 8. *A*: Ba^{2+} current (I_{Ba}) traces of rat brain 1C subunit (rbCII) and the DA variant. Peak normalized currents were averaged and superimposed. Pulse protocol is indicated above current traces. *B*: voltage dependence of I_{Ba} density of DA variant and rbCII. *C*: current-voltage (*I-V*) relations (curve) of rbCII and the DA variant. Amplitude of I_{Ba} was normalized to peak value in each recording and averaged. *D*: steady-state inactivation curves of rbCII and the DA variant. Test pulse to 0 mV for 100 ms was applied after conditioning pulse for 5 s to the respective voltages ranging from −80 to 10 mV in 10-mV steps and for 25 ms at −70 mV. Values are means ± SE.

ing. Although the abundant expression of the α_{1G}-subunit suggests that the α_{1G}-subunit plays an important role in the DA, the physiological role of T-type VDCCs in smooth muscle contraction has been obscure. However, Ca^{2+} influx through the α_{1H}-subunit has been recently identified to be essential for normal relaxation of coronary arteries (4). Therefore, T-type VDCCs may play a similar role in the DA, rather than in oxygen-sensitive contraction (38). Further investigation is necessary to test the possibility.

In addition to the regulation of vascular tone, L- and T-type VDCCs are also known to regulate differentiation (14, 17), proliferation (19, 36, 44), migration (7, 31), and gene expression (41) in vascular SMCs. In the present study, we found that L- and T-type Ca^{2+} channel blockers significantly inhibited [^{3}H]thymidine incorporation in DA SMCs, suggesting that L- and T-type VDCCs promote cell proliferation in the DA. Moreover, we found that BAY K 8644, an L-type VDCC activator, increased DA SMC migration in a dose-dependent manner (unpublished data). A previous study demonstrated that the blockade of T-type, but not L-type, VDCCs prevented neointima formation after vascular injury (32), which shares a molecular mechanism of intimal thickening similar to that of the DA. Our present results, however, indicate that L- and T-type VDCCs are involved in intimal thickening in the DA in different ways.

Previous studies demonstrated that responses of the DA to oxygen and indomethacin, a prostaglandin H synthase inhibitor, are blunted at e19 and are apparent at e21 (24, 25). In this study, the expression level of α_{1C}-subunit mRNA at e19 was similar to that at e21 or *day 0*. Therefore, the expression level of the α_{1C}-subunit was not considered the cause of the blunted response of the DA to oxygen and indomethacin at e19. One may argue that an oxygen-sensitive signal is activated at near term (e21) to increase the activity of VDCCs. In this sense, vitamin A and/or retinoic acid signaling is a candidate for the activator of oxygen sensitivity, because the retinoic acid response element is strongly expressed in the mouse DA (6), and maternally administered vitamin A accelerated development of the oxygen-sensing mechanism of the rat DA (42). Previous studies have also demonstrated that retinoic acid upregulated α_{1C}-subunit L-type Ca^{2+} channel expression in vascular SMCs (13) and H_9C_2 cardiac myoblast cell lines (22). Although vitamin A upregulated the expression of α_{1C}-subunit mRNA in the DA only at *day 0*, it would be of great interest that vitamin A and/or retinoic acid signal may enhance the activity of VDCCs in the DA.

We found a novel spliced variant of the α_{1C}-subunit in the rat. The spliced variant contained a 25-amino acid insertion into the I-II cytoplasmic linker. The interaction between the cytoplasmic I-II linker of α_{1C}- and β-subunits is known to modulate channel opening (16). During the preparation of this manuscript, Liao et al. (18) reported the same spliced variant of the α_{1C}-subunit. They demonstrated that the spliced variant of the α_{1C}-subunit exhibited a hyperpolarized shift in voltage-dependent activation and the *I-V* relation in HEK 293 cells. However, we did not find a difference in basic electrophysiological channel properties between the conventional and the spliced variant of α_{1C}-subunits. Although we do not explain an exact reason for the conflicting results between two studies, the discrepancy may be due to the different conditions of the experiments: we used rat cDNA and the β_1-subunit, whereas Liao et al. used human cDNA and the β_2-subunit. Although we did not find a difference in basic channel properties between the conventional and the spliced variant of α_{1C}-subunits, we found the distinct expression pattern of the spliced variant in the DA. The spliced variant was strongly expressed in neointimal thickening of the DA, where SMCs exhibit more proliferating and migrating characters (33, 34). In addition, we found that expression of the spliced variant mRNA was significantly increased in the lung of monocrotaline-treated rats (unpublished data). These results suggest a distinct role for the spliced variant in adaptation to various physiological and/or pathological signals.

In conclusion, multiple VDCC subunits were identified in the DA, and, in particular, α_{1C}- and α_{1G}-subunits were predominant in the DA. The expression of α_{1C}- and α_{1G}-subunit mRNAs was higher in the DA than in the aorta and was significantly upregulated by maternal administration of vitamin A. We found a novel spliced variant of the α_{1C}-subunit gene that may play a specific role in Ca^{2+} entry in the lung and fetal arteries. Our study could be an important first step in identification of the molecular basis of Ca^{2+} channel function in the DA. On the basis of our results, further study would identify the physiological relevance between mRNA levels and Ca^{2+} channel function in the DA.

ACKNOWLEDGMENTS

We are grateful to Takayo Musuda, Mayumi Watanabe, and Chikako Usami for excellent technical assistance and animal care. Efonidipine was kindly provided by Nissan Chemical Industries (Saitama, Japan).

GRANTS

This work was partly supported by the Mother and Child Health Foundation (S. Minamisawa), 2005 Strategic Research Project Grant K17014 of Yokohama City University (S. Minamisawa), the Yokohama Foundation for Advancement of Medical Science (U. Yokoyama and T. Akaike), and a Grant-in-Aid for Scientific Research from the Japanese Society for the Promotion of Science (S. Adachi-Akahane).

REFERENCES

1. **Arikkath J and Campbell KP.** Auxiliary subunits: essential components of the voltage-gated calcium channel complex. *Curr Opin Neurobiol* 13: 298–307, 2003.
2. **Bijlenga P, Liu JH, Espinos E, Haenggeli CA, Fischer-Lougheed J, Bader CR, and Bernheim L.** T-type α_{1H} Ca^{2+} channels are involved in Ca^{2+} signaling during terminal differentiation (fusion) of human myoblasts. *Proc Natl Acad Sci USA* 97: 7627–7632, 2000.
3. **Catterall WA.** Structure and regulation of voltage-gated Ca^{2+} channels. *Annu Rev Cell Dev Biol* 16: 521–555, 2000.
4. **Chen CC, Lamping KG, Nuno DW, Barresi R, Prouty SJ, Lavoie JL, Cribbs LL, England SK, Sigmund CD, Weiss RM, Williamson RA, Hill JA, and Campbell KP.** Abnormal coronary function in mice deficient in α_{1H} T-type Ca^{2+} channels. *Science* 302: 1416–1418, 2003.
5. **Coceani F and Olley PM.** The control of cardiovascular shunts in the fetal and perinatal period. *Can J Physiol Pharmacol* 66: 1129–1134, 1988.
6. **Colbert MC, Kirby ML, and Robbins J.** Endogenous retinoic acid signaling colocalizes with advanced expression of the adult smooth muscle myosin heavy chain isoform during development of the ductus arteriosus. *Circ Res* 78: 790–798, 1996.
7. **Corsini A, Bonfatti M, Quarato P, Accomazzo MR, Raiteri M, Sartani A, Testa R, Nicosia S, Paoletti R, and Fumagalli R.** Effect of the new calcium antagonist lercanidipine and its enantiomers on the migration and proliferation of arterial myocytes. *J Cardiovasc Pharmacol* 28: 687–694, 1996.
8. **Davis MJ and Hill MA.** Signaling mechanisms underlying the vascular myogenic response. *Physiol Rev* 79: 387–423, 1999.
9. **Del Toro R, Levitsky KL, Lopez-Barneo J, and Chiara MD.** Induction of T-type calcium channel gene expression by chronic hypoxia. *J Biol Chem* 278: 22316–22324, 2003.
10. **De Reeder EG, Poelmann RE, van Munsteren JC, Patterson DF, and Gittenberger-de Groot AC.** Ultrastructural and immunohistochemical changes of the extracellular matrix during intimal cushion formation in the ductus arteriosus of the dog. *Atherosclerosis* 79: 29–40, 1989.
11. **Fearon IM, Varadi G, Koch S, Isaacsohn I, Ball SG, and Peers C.** Splice variants reveal the region involved in oxygen sensing by recombinant human L-type Ca^{2+} channels. *Circ Res* 87: 537–539, 2000.
12. **Ferron L, Capuano V, Deroubaix E, Coulombe A, and Renaud JF.** Functional and molecular characterization of a T-type Ca^{2+} channel during fetal and postnatal rat heart development. *J Mol Cell Cardiol* 34: 533–546, 2002.
13. **Gollasch M, Haase H, Ried C, Lindschau C, Morano I, Luft FC, and Haller H.** L-type calcium channel expression depends on the differentiated state of vascular smooth muscle cells. *FASEB J* 12: 593–601, 1998.
14. **Gollasch M, Lohn M, Furstenau M, Nelson MT, Luft FC, and Haller H.** Ca^{2+} channels, "quantized" Ca^{2+} release, and differentiation of myocytes in the cardiovascular system. *J Hypertens* 18: 989–998, 2000.
15. **Hofmann F, Lacinova L, and Klugbauer N.** Voltage-dependent calcium channels: from structure to function. *Rev Physiol Biochem Pharmacol* 139: 33–87, 1999.
16. **Hohaus A, Poteser M, Romanin C, Klugbauer N, Hofmann F, Morano I, Haase H, and Groschner K.** Modulation of the smooth-muscle L-type Ca^{2+} channel α_1 subunit ($\alpha_{1C\text{-}b}$) by the β_{2a} subunit: a peptide which inhibits binding of β to the I-II linker of α_1 induces functional uncoupling. *Biochem J* 348: 657–665, 2000.
17. **Kuga T, Kobayashi S, Hirakawa Y, Kanaide H, and Takeshita A.** Cell cycle-dependent expression of L- and T-type Ca^{2+} currents in rat aortic smooth muscle cells in primary culture. *Circ Res* 79: 14–19, 1996.
18. **Liao P, Yu D, Lu S, Tang Z, Liang MC, Zeng S, Lin W, and Soong TW.** Smooth muscle-selective alternatively spliced exon generates functional variation in $Ca_v1.2$ calcium channels. *J Biol Chem* 279: 50329–50335, 2004.
19. **Lijnen P, Fagard R, and Petrov V.** Mibefradil-induced inhibition of proliferation of human peripheral blood mononuclear cells. *J Cardiovasc Pharmacol* 33: 595–604, 1999.
20. **McCleskey EW.** Calcium channels: cellular roles and molecular mechanisms. *Curr Opin Neurobiol* 4: 304–312, 1994.
21. **McCobb DP, Best PM, and Beam KG.** Development alters the expression of calcium currents in chick limb motoneurons. *Neuron* 2: 1633–1643, 1989.
22. **Menard C, Pupier S, Mornet D, Kitzmann M, Nargeot J, and Lory P.** Modulation of L-type calcium channel expression during retinoic acid-induced differentiation of H9C2 cardiac cells. *J Biol Chem* 274: 29063–29070, 1999.
23. **Minamisawa S, Oshikawa J, Takeshima H, Hoshijima M, Wang Y, Chien KR, Ishikawa Y, and Matsuoka R.** Junctophilin type 2 is associated with caveolin-3 and is down-regulated in the hypertrophic and dilated cardiomyopathies. *Biochem Biophys Res Commun* 325: 852–856, 2004.
24. **Momma K, Nakanishi T, and Imamura S.** Inhibition of in vivo constriction of fetal ductus arteriosus by endothelin receptor blockade in rats. *Pediatr Res* 53: 479–485, 2003.
25. **Momma K, Toyono M, and Miyagawa-Tomita S.** Accelerated maturation of fetal ductus arteriosus by maternally administered vitamin A in rats. *Pediatr Res* 43: 629–632, 1998.
26. **Moosmang S, Schulla V, Welling A, Feil R, Feil S, Wegener JW, Hofmann F, and Klugbauer N.** Dominant role of smooth muscle L-type calcium channel $Ca_v1.2$ for blood pressure regulation. *EMBO J* 22: 6027–6034, 2003.
27. **Naguro I, Nagao T, and Adachi-Akahane S.** Ser^{1901} of α_{1C} subunit is required for the PKA-mediated enhancement of L-type Ca^{2+} channel currents but not for the negative shift of activation. *FEBS Lett* 489: 87–91, 2001.
28. **Nakanishi T, Gu H, Hagiwara N, and Momma K.** Mechanisms of oxygen-induced contraction of ductus arteriosus isolated from the fetal rabbit. *Circ Res* 72: 1218–1228, 1993.
29. **Plant TD, Schirra C, Katz E, Uchitel OD, and Konnerth A.** Single-cell RT-PCR and functional characterization of Ca^{2+} channels in motoneurons of the rat facial nucleus. *J Neurosci* 18: 9573–9584, 1998.
30. **Rabinovitch M.** Cell-extracellular matrix interactions in the ductus arteriosus and perinatal pulmonary circulation. *Semin Perinatol* 20: 531–541, 1996.
31. **Ruiz-Torres A, Lozano R, Melon J, and Carraro R.** L-calcium channel blockade induced by diltiazem inhibits proliferation, migration and F-actin membrane rearrangements in human vascular smooth muscle cells stimulated with insulin and IGF-1. *Int J Clin Pharmacol Ther* 41: 386–391, 2003.
32. **Schmitt R, Clozel JP, Iberg N, and Buhler FR.** Mibefradil prevents neointima formation after vascular injury in rats. Possible role of the blockade of the T-type voltage-operated calcium channel. *Arterioscler Thromb Vasc Biol* 15: 1161–1165, 1995.
33. **Slomp J, Gittenberger-de Groot AC, Glukhova MA, Conny van Munsteren J, Kockx MM, Schwartz SM, and Koteliansky VE.** Differentiation, dedifferentiation, and apoptosis of smooth muscle cells during the development of the human ductus arteriosus. *Arterioscler Thromb Vasc Biol* 17: 1003–1009, 1997.
34. **Slomp J, Gittenberger-de Groot AC, Koteliansky VE, Glukhova MA, Bogers AJ, and Poelmann RE.** Cytokeratin expression in human arteries

pertinent to intimal thickening formation in the ductus arteriosus. *Differentiation* 61: 305–311, 1997.

35. **Snutch TP, Tomlinson WJ, Leonard JP, and Gilbert MM.** Distinct calcium channels are generated by alternative splicing and are differentially expressed in the mammalian CNS. *Neuron* 7: 45–57, 1991.
36. **Sperti G and Colucci WS.** Calcium influx modulates DNA synthesis and proliferation in A7r5 vascular smooth muscle cells. *Eur J Pharmacol* 206: 279–284, 1991.
37. **Takizawa T, Oda T, Arishima K, Yamamoto M, Masaoka T, Somiya H, Akahori F, and Shiota K.** A calcium channel blocker verapamil inhibits the spontaneous closure of the ductus arteriosus in newborn rats. *J Toxicol Sci* 19: 171–174, 1994.
38. **Tristani-Firouzi M, Reeve HL, Tolarova S, Weir EK, and Archer SL.** Oxygen-induced constriction of rabbit ductus arteriosus occurs via inhibition of a 4-aminopyridine-, voltage-sensitive potassium channel. *J Clin Invest* 98: 1959–1965, 1996.
39. **Tsien RW, Lipscombe D, Madison DV, Bley KR, and Fox AP.** Multiple types of neuronal calcium channels and their selective modulation. *Trends Neurosci* 11: 431–438, 1988.
40. **Uemura N, Ohkusa T, Hamano K, Nakagome M, Hori H, Shimizu M, Matsuzaki M, Mochizuki S, Minamisawa S, and Ishikawa Y.** Down-regulation of sarcolipin mRNA expression in chronic atrial fibrillation. *Eur J Clin Invest* 34: 723–730, 2004.
41. **Wamhoff BR, Bowles DK, McDonald OG, Sinha S, Somlyo AP, Somlyo AV, and Owens GK.** L-type voltage-gated Ca^{2+} channels modulate expression of smooth muscle differentiation marker genes via a Rho kinase/myocardin/SRF-dependent mechanism. *Circ Res* 95: 406–414, 2004.
42. **Wu GR, Jing S, Momma K, and Nakanishi T.** The effect of vitamin A on contraction of the ductus arteriosus in fetal rat. *Pediatr Res* 49: 747–754, 2001.
43. **Yamaguchi S, Okamura Y, Nagao T, and Adachi-Akahane S.** Serine residue in the IIIS5-S6 linker of the L-type Ca^{2+} channel α_{1C} subunit is the critical determinant of the action of dihydropyridine Ca^{2+} channel agonists. *J Biol Chem* 275: 41504–41511, 2000.
44. **Yang Z, Noll G, and Luscher TF.** Calcium antagonists differently inhibit proliferation of human coronary smooth muscle cells in response to pulsatile stretch and platelet-derived growth factor. *Circulation* 88: 832–836, 1993.

Compounds Structurally Related to Tamoxifen as Openers of Large-Conductance Calcium-Activated K^+ Channel

Yu SHA,[a,b] Toshihiko TASHIMA,[a] Yumi MOCHIZUKI,[a] Yoshimi TORIUMI,[a] Satomi ADACHI-AKAHANE,[a] Taro NONOMURA,[a] Maosheng CHENG,[b] and Tomohiko OHWADA*[,a]

[a] *Graduate School of Pharmaceutical Sciences, The University of Tokyo; Hongo, Bunkyo-ku, Tokyo 113–0033, Japan: and* [b] *Shenyang Pharmaceutical University; 103 Wenhua Road, Shenyang, Liaoning, 110016, P.R. China.* Received July 26, 2005; accepted August 18, 2005; published online August 22, 2005

We found that a variety of compounds containing partial structures of tamoxifen showed activity as chemical modulators of large-conductance calcium-activated K^+ channels (BK channels).

Key words large-conductance calcium-activated K^+ channel; tamoxifen; channel opener; (xeno)estrogen; electrophysiology

Large-conductance calcium-activated K^+ channels (BK channels) characteristically respond to two distinct physiological stimuli, *i.e.*, changes in membrane voltage and in cytosolic Ca^{2+} concentration.[1] The BK channel opens in response to an increase in cytosolic Ca^{2+} concentration and membrane depolarization, resulting in an increase of K^+ efflux, which leads to rapid hyperpolarization of the excitatory membrane and thus reduces Ca^{2+} influx through voltage-dependent Ca^{2+} channels. The BK channel is formed by a tetramer of the pore-forming α-subunit and up to four β-subunits that function to modulate the BK channel.[2,3] Recent cloning studies also revealed the presence of multiple splice variants of α-subunits[4—6] and multiple subtypes of β-subunits (β_1, β_2/β_3 and β_4).[7—9] Thus, there is a large diversity of BK channels, which may be specific to tissues and organs.[4—6] Except for cardiac myocytes, the BK channels are expressed in a number of organ systems, such as smooth muscle cells, skeletal muscle cells, neuronal cells, and secretary epithelial cells,[10] and they have important physiological roles in modulating muscle contraction and neuronal activities, such as synaptic transmission.[11]

These features and the widespread distribution of the channel throughout the central nervous system and in peripheral tissues offer rich opportunities for discovering novel therapeutic agents based on BK channel modulators, particularly openers.[12,13] Chemical channel openers are expected to quench excitatory events that pathologically elevate the cytosolic Ca^{2+} and induce depolarization of the cell membranes, and potentially have specificity for tissues and organs of interest. Well-characterized BK channel openers could be used to treat acute stroke, epilepsy, and bladder overactivity.[14] There is some evidence for the utility of BK channel openers in the treatment of asthma, hypertension, gastric hypermotility and psychoses.[1] Recent studies have shown that the BK channel is one of the targets for the non-genomic effects of (xeno)estrogens, such as tamoxifen and estradiol.[15—19] The stimulatory action of tamoxifen and 17β-estradiol on the BK channel activity requires the presence of the β_1 subunit.[15—19] Herein, we show that compounds containing partial structures of tamoxifen can activate the human BK channels, possibly through action on the β_1 subunit.

Compounds **3a—o** were synthesized by means of McMurry condensation reaction of a substituted benzophenone derivative and 3-pentanone in the presence of $TiCl_4$ and zinc powder in dry THF with heating at reflux for 4—20 h.[20] Preliminary assay by using the fluorescent dye method with $DiBAC_4(3)$ was applied with rat rSlo α and β_1 stably expressing human embryonic kidney (HEK 293) cell lines.[21] The results are shown in Fig. 1. The magnitude of release of the dye from the inside of the cells upon opening of the BK channels is shown in terms of the normalized decrease of fluorescence of the dye, relative to that in the case of tamoxifen, defined as 100 (%). The observed relative magnitudes were based on a large set of data (n=11—19). The larger the value, the stronger the opening activity of a compound. As shown in Fig. 1, the *N*,*N*-dimethylaminoethyloxy group of tamoxifen is not necessary for activity (see **3a**). The acidic phenol functionality is also not essential, but rather hydrophobicity, such as a methoxy (**3c**) or trifluoromethyl group (**3h**), is crucial, particularly at the *para* position. Compounds in which the two benzenes are substituted are less potent (**3l—o**). While diethylstilbestrol (DES) is more potent than tamoxifen in the dye assay, 4,4′-dimethoxystilbene, **4a**, is more potent than the present series of the compounds **3a—o**. In DES and **4a**, the arrangement of the two benzenes with

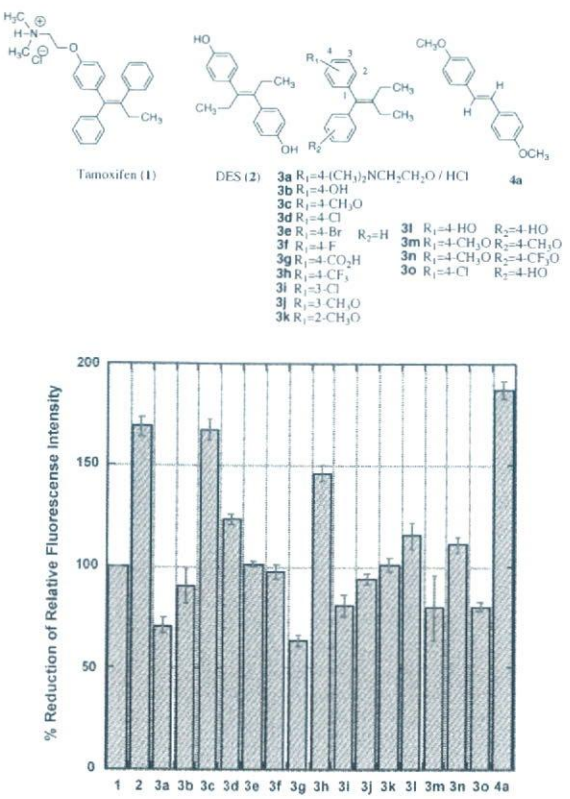

Fig. 1. Fluorescent Dye Assay Result
n=11—19.

* To whom correspondence should be addressed. e-mail: ohwada@mol.f.u-tokyo.ac.jp

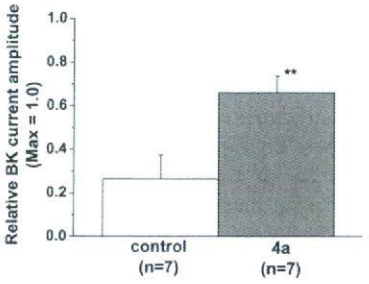

Fig. 2. Electrophysiological Effect of **4a** on the BK Channel Current

Vehicle containing DMSO at 0.05—0.1% was used as control. Statistical analysis was performed with Student's *t*-test. $p<0.05$ was accepted as statistically significant (**).

respect to the central double bond is different from that in **3a**—**o**.

We further investigated the channel opening activity of **4a** electrophysiologically (Fig. 2).

The BK channel currents were recorded by the inside-out patch-clamp technique from HEK-293 cells expressing human hSlo α and β_1 subunits.[22] We also repeated the same experiment with rSlo α and β_1 subunits. Compound **4a** apparently increased the relative current amplitude, activated by the test potential to 120 mV from the holding potential of −60 mV, as compared with the control. **4a** did not show significant effects when hSlo α was expressed without β_1 subunit (data not shown). The half activation potential was shifted from 136.5±4.9 mV (n=7) to 120±6.1 mV (n=7) by **4a**, indicating that the BK channel activity was facilitated by **4a**. Clearly, a hydroxyl group on the aromatic ring is not essential for the BK channel opening activity of the tamoxifen derivatives. Thus, the present work suggests a simple but important criterion for the design of tamoxifen derivatives as BK channel openers.

Acknowledgments This work was supported by a Grant-in-Aid for Scientific Research from the Ministry of Health, Labour and Welfare (H17-Chemistry-006) to T. O. and S. A.-A. A scholarship, provided by the 21st Century Center of Excellence (COE) Program (Japan Society for the Promotion of Sciences) to Y. S. and T. T. is also gratefully acknowledged. We also thank Prof. Yuji Imaizumi, Nagoya City University, Nagoya, Japan, for the gift of the rSlo α and β_1 stably expressing HEK cells. We also appreciate the gift of hslo α and β_1 from Prof. Ligia Toro, The University of California at Los Angeles.

References

1) Gribkoff V. K., Starrett J. E., Jr., Droretzky S. I., "Advances in Pharmacology," Vol. 37, ed. by Augst J. T., Anders M. W., Murad F., Coyle J. T., Academic Press, San Diego, 1997, pp. 319—349.
2) Niu X., Magleby K. L., *Proc. Natl. Acad. Sci. U.S.A.*, **99**, 11441—11446 (2002).
3) Jiang Y., Lee A., Chen J., Cadene M., Chalt B. T., MacKinnon R., *Nature* (London), **417**, 515—522 (2002).
4) Garica-Calvo M., Knaus H.-G., McManus O. B., Giangiacomo K. M., Kaczorowski G. J., Garcia M. L., *J. Biol. Chem.*, **269**, 676—682 (1994).
5) Tian L., Duncan R. R., Hammond M. S., Coghill L. S., Wen H., Rusinova R., Clark A. G., Levitan I. B., Shipston M. J., *J. Biol. Chem.*, **276**, 7717—7720 (2001).
6) Zarei M. M., Eghbali M., Alioua A., Song M., Knaus H. G., Stefani E., Toro L., *Proc. Natl. Acad. Sci. U.S.A.*, **101**, 10072—10077 (2004).
7) Knaus H.-G., Folander K., Garcia-Calvo M., Garcia M. L., Kaczorowski G. J., Smith M., Swanson R., *J. Biol. Chem.*, **269**, 17274—17278 (1994).
8) Tanaka Y., Koike K., Alioua A., Shigenobu K., Stefani E., Taro L., *J. Pharmacol. Sci.*, **94**, 339—347 (2004).
9) Tseng-Crank J., Godinot N., Johansen T. E., Ahring P. K., Strøbæk D., Mertz R., Foster C. D., Olesen S.-P., Reinhart P. H., *Proc. Natl. Acad. Sci. U.S.A.*, **93**, 9200—9205 (1996).
10) Knaus H.-G., Schwarzer C., Koch R. O. A., Eberhart A., Kaczorowski G. J., Glossmann H., Wunder F., Pongs O., Garcia M. L., Sperk G., *J. Neurosci.*, **16**, 955—963 (1996).
11) Sah P., Faber E. S. L., *Prog. Neurobio.*, **66**, 345—353 (2002).
12) Coghlan M. J., Carroll W. A., Gopalakrishnan M., *J. Med. Chem.*, **44**, 1627—1653 (2001).
13) Shieh C.-C., Coghlan M., Sullivan J. P., Gopalakrishnan M., *Pharmacol. Rev.*, **52**, 557—593 (2000).
14) Gribkoff V. K., Starrett J. E., Jr., Dworetzky S. I., Hewawasam P., Boissard C. G. J. R., Huston K., Johnson G., Krishman B. S., Kinney G. G., Lombardo L. A., Meanwell N. A., Molinoff P. B., Myers R. A., Moon S. L., Ortiz A., Pajor L., Pieschl R. L., Post-Munson D. J., Signor L. J., Srinivas N., Taber M. T., Thalody G., Trojnacki J. T., Wiener H., Yeleswarm K., Yeola S. W., *Nature Medicine*, **7**, 471—477 (2001).
15) Tamoxifen derivatives: Valverde M. A., Rojas P., Amigo J., Cosmelli D., Orio P., Bahamonde M. I., Mann G. E., Vergara C., Latorre R., *Science*, **285**, 1929—1931 (1999).
16) Tamoxifen derivatives: Dick G. M., Rossow C. F., Smirnov S., Horowitz B., Sanders K. M., *J. Biol. Chem.*, **276**, 34594—34599 (2001).
17) Tamoxifen derivatives: Dick G. M., Sanders K. M., *J. Biol. Chem.*, **276**, 44835—44840 (2001).
18) Tamoxifen derivatives: Dick G. M., Hunter A. C., Sanders K. M., *Mol. Pharmacol.*, **61**, 1105—1113 (2002).
19) Dunncan R. K., *Biochem. Pharmacol.*, **70**, 47—58 (2005).
20) McMurry coupling: Detsi A., Koufaki M., Calogeropoulou T., *J. Org. Chem.*, **67**, 4608—4611 (2002).
21) Yamada A., Gaja N., Ohya S., Muraki K., Narita H., Ohwada T., Imaizumi Y., *Jpn. J. Pharmacol.*, **86**, 342—350 (2001).
22) Nishimaru K., Eghbali M., Lu R., Marijic J., Stefani E., Toro L., *J. Physiol.*, **559**, 849—862 (2004).

Available online at www.sciencedirect.com

SCIENCE DIRECT

European Journal of Pharmacology 508 (2005) 23–30

www.elsevier.com/locate/ejphar

Characterization of voltage-dependent gating of $P2X_2$ receptor/channel

Ken Nakazawa[a,*], Yasuo Ohno[b]

[a]*Cellular and Molecular Pharmacology Section, Division of Pharmacology, National Institute of Health Sciences, 1-18-1 Kamiyoga, Setagaya, Tokyo 158-8501, Japan*

[b]*Division of Pharmacology, National Institute of Health Sciences, 1-18-1 Kamiyoga, Setagaya, Tokyo 158-8501, Japan*

Received 9 September 2004; received in revised form 29 November 2004; accepted 6 December 2004
Available online 4 January 2005

Abstract

The role of a voltage-dependent gate of recombinant $P2X_2$ receptor/channel was investigated in *Xenopus* oocytes. When a voltage step to −110 mV was applied from a holding potential of −50 mV, a gradual increase was observed in current evoked by 30 μM ATP. Contribution of this voltage-dependent component to total ATP-evoked current was greater when the current was evoked by lower concentrations of ATP. The voltage-dependent gate closed upon depolarization, and half the gates were closed at −80 mV. On the other hand, a potential at which half the gates opened was about −30 mV or more positive, which was determined using a series of hyperpolarization steps. The results of the present study suggest that the voltage-dependent gate behavior of $P2X_2$ receptor is not due to simple activation and deactivation of a single gate, but rather due to transition from a low to a high ATP affinity state.

Keywords: P2X receptor; Voltage dependence; Gate; Kinetics; Ligand affinity

1. Introduction

Extracellular ATP is considered a neurotransmitter, and its fast neurotransmission is mediated through ion channel-forming P2X receptors (see reviews, Ralevic and Burnstock, 1998; Khakh, 2001; North, 2002). To date, at least seven subclasses of P2X receptor ($P2X_{1-7}$) have been cloned, which form homo- or heteromeric receptors that act as functional ion channels (North and Surprenant, 2000). Each subclass consists of two transmembrane domains (TM1 and TM2) and one long extracellular domain (E1) between them. Both TM1 (Jiang et al., 2001; Haines et al., 2001) and TM2 (Rassendren et al., 1997; Egan et al., 1998; Migita et al., 2001) contribute to formation of the channel pore. P2X receptor/channels are permeable to cations, but demonstrate poor cation selectivity. The channels are gated by ATP molecules, and the narrowest part of the channel pore opens when activated (Rassendren et al., 1997). The ATP-binding site for gating is partly attributable to basic amino acid residues near the outer mouth of the channel pore formed by TM1 and TM2 (Ennion et al., 2000; Jiang et al., 2000), and the possibility that aromatic residues in E1 contribute to the binding site has also been suggested (Nakazawa et al., 2002; Roberts and Evans, 2004).

In addition to ATP, other factors are known to modulate channel activity. Zn^{2+} and acidic conditions facilitate ATP-mediated gating by increasing ATP sensitivity of $P2X_2$ receptor (Clyne et al., 2002). Neurotransmitters, including dopamine, and related compounds also facilitate ATP-mediated gating (Nakazawa et al., 1997a). Membrane potential may also play a role. It has been reported that ionic current activated by ATP is enhanced by hyperpolarization in pheochromocytoma PC12 cells (Nakazawa et al., 1997b). We observed similar voltage-dependent gating of recombinant $P2X_2$ receptor/channel, which was originally cloned from PC12 cells (Brake et al., 1994), and qualitatively analyzed its properties in the present study.

2. Methods

Recordings of ionic current through recombinant $P2X_2$ receptor/channels were performed according to our previous

* Corresponding author. Tel.: +81 3 3700 9704; fax: +81 3 3707 6950.
E-mail address: nakazawa@nihs.go.jp (K. Nakazawa).

0014-2999/$ - see front matter © 2004 Elsevier B.V. All rights reserved.
doi:10.1016/j.ejphar.2004.12.005

report (Nakazawa and Ohno, 1997). Briefly, the cloned rat $P2X_2$ receptor (Brake et al., 1994) was expressed in *Xenopus* oocytes by injecting in vitro transcribed cRNA. After 4 days of incubation at 18 °C, the membrane current of the oocytes was recorded. Oocytes were bathed in ND96 solution containing (in mM) NaCl 96, KCl 2, $CaCl_2$ 1.8, $MgCl_2$ 1, HEPES 5 (pH 7.5 with NaOH). In some experiments, oocytes were bathed in solution containing 10.8 mM $BaCl_2$ instead of 1.8 mM $CaCl_2$. When achieving a low extracellular chloride concentration, 96 mM Na-acetate was added instead of 96 mM NaCl. ATP (adenosine 5′ -triphosphate disodium salt; Sigma, St. Louis, MO, U.S.A.) was applied by superfusion for approximately 10 s at regular 2-min intervals. Membrane current was recorded using the standard two-electrode voltage-clamp techniques, and electrical signals were stored on a data recorder (PC204Ax; SONY, Tokyo, Japan) for off-line analysis. Curve fittings to data were made using Microsoft' Excel X.

3. Results

3.1. Voltage-dependent component of ATP-evoked current

Fig. 1A compares membrane currents in the absence and presence of 30 μM ATP in a $P2X_2$ receptor-expressing oocyte. The oocyte was held at −50 mV and stepped to −110 mV for 200 ms. In the presence of ATP, inward current at −110 mV did not instantaneously reach steady-state, but gradually increased: a biphasic increase in current was observed with a voltage-independent component ("a" in Fig. 1A) and a voltage-dependent component ("b" in Fig. 1A). When the voltage was returned to −50 mV, a gradually declining inward "tail" current was observed ("c" in Fig. 1A). The voltage-dependent component of the inward current at −110 mV was observed to follow first-order kinetics with a time constant of 40 ms (Fig. 1B).

Fig. 2A demonstrates an increased magnitude of the voltage-dependent component when activated from a less negative holding potential. The voltage-dependent component was larger when the step to −110 mV was applied from −10 mV ("a" in Fig. 2A) than when it was applied from −70 mV ("b" in Fig. 2A). This dependence of the voltage-dependent component on holding potentials is illustrated in Fig. 2B. It is worth noting that Ca^{2+}-activated currents exist in *Xenopus* oocytes (Weber, 1999; Zhang and Hamill, 2000). Since P2X receptor/channels are Ca^{2+}-permeable (Khakh, 2001), a secondarily activated Ca^{2+}-induced current might contribute to the observed voltage-dependent changes. This does not, however, appear to be the case since a similar dependence on holding potentials was observed when extracellular Ca^{2+} was replaced with 10.8 mM Ba^{2+}. Time constants for the activation of the voltage-dependent component were obtained as shown in Fig. 1B, and the mean values were plotted against holding potentials

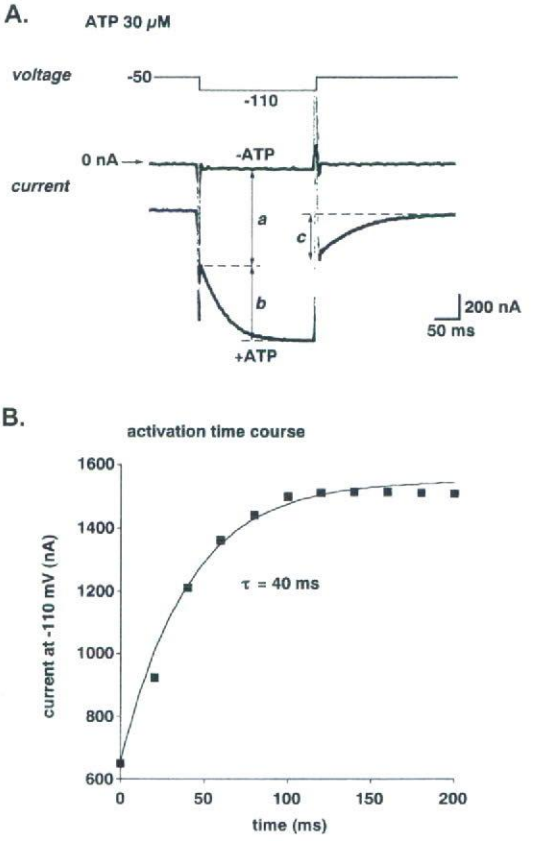

Fig. 1. (A) Current traces of an oocyte stepped to −110 mV from a holding potential of −50 mV in the absence (−ATP) or presence (+ATP) of 30 μM ATP. The current evoked by ATP is represented by the difference between the two traces. Upon hyperpolarization, a gradual increase in current was observed in the presence of ATP, suggesting activation of a voltage-dependent gate (denoted by "b"). The current denoted by "c" represents a gradually declining "tail current" that was observed when the voltage was returned to −50 mV. (B) Time course of activation of the voltage-dependent component. Current amplitude of the voltage-dependent component represented by "b" in panel A was plotted against time after the onset of hyperpolarization at −110 mV. The voltage-dependent component could be made to fit a curve with a time constant of 40 ms.

(Fig. 2C). While the current amplitude demonstrated voltage dependence (Fig. 2B), voltage did not have an effect on time course of the activation.

3.2. Effect of ATP concentrations

Fig. 3A shows the voltage-dependent component of the current activated by 10 μM or 300 μM of ATP in a single oocyte. The relative size of the voltage-dependent component involved in total ATP-evoked current became smaller when the current was evoked by greater concentrations of ATP (Fig. 3A and B). A similar dependence on ATP concentration was observed for the current evoked in the presence of 10.8 mM Ba^{2+} instead of 1.8 mM Ca^{2+} (Fig. 3B). Dependence on ATP concentrations was also found for activation time constants for the voltage-

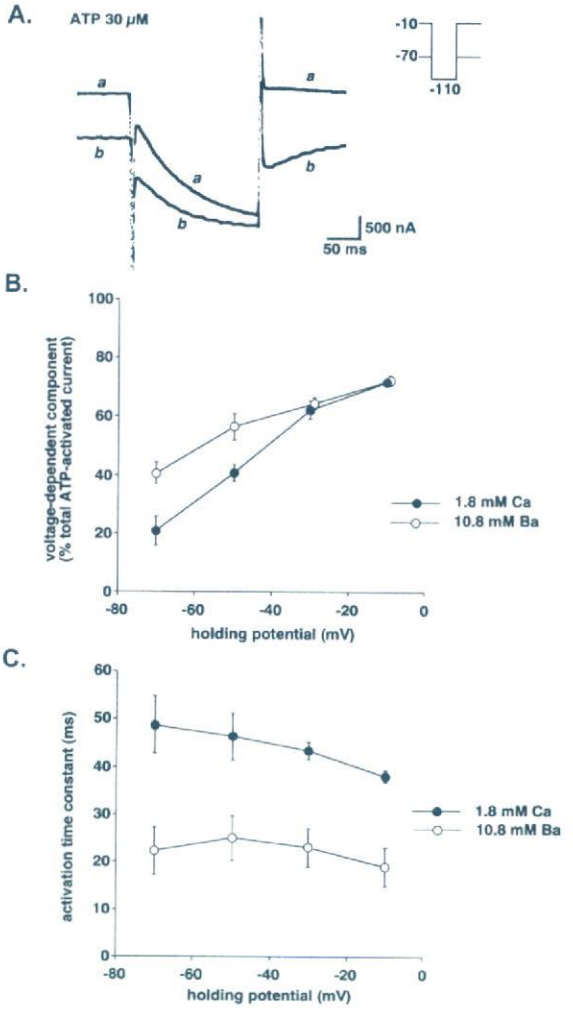

Fig. 2. Effect of holding potential on current. Current was evoked by 30 μM ATP. (A) Voltage-dependent current at −110 mV when stepped from a holding potential of −10 mV ("a") or −70 mV ("b"). (B) Effect of holding potential on voltage-dependent current. The amplitude of the voltage-dependent current was measured as described in Fig. 1A. Mean values obtained from 4 oocytes in a standard extracellular solution containing 1.8 mM Ca^{2+} (●) and an extracellular solution containing 10.8 mM Ba^{2+} (instead of Ca^{2+}; ○) were plotted. Bars represent the S.E.M. (C) Time course of activation of the voltage-dependent component. Time constants were determined as shown in Fig. 1B, and mean values obtained from 4 oocytes were plotted against holding potentials. Bars represent the S.E.M.

dependent component; the time constants were larger for 10 μM ATP than 30 μM ATP (Fig. 3C).

3.3. Activation and deactivation kinetics

Cl^- currents are observed in *Xenopus* oocytes (Weber, 1999; Zhang and Hamill, 2000). In the following experiments, current measurements were made using an extracellular solution containing 96 mM Na-aspartate instead of NaCl in order to facilitate the analysis of the voltage-dependent component of ATP-evoked current by reducing Cl^- currents. In doing so, there was an obvious reduction in outward current upon depolarization, resulting in better voltage-clamp conditions. Using this extracellular solution, the EC_{50} value for ATP-activated current measured at −50 mV was about 40 μM, which was lower than the value obtained with the standard extracellular solution containing 96 mM NaCl (about 100 μM; Nakazawa and Ohno, 2004). Fig. 4 illustrates

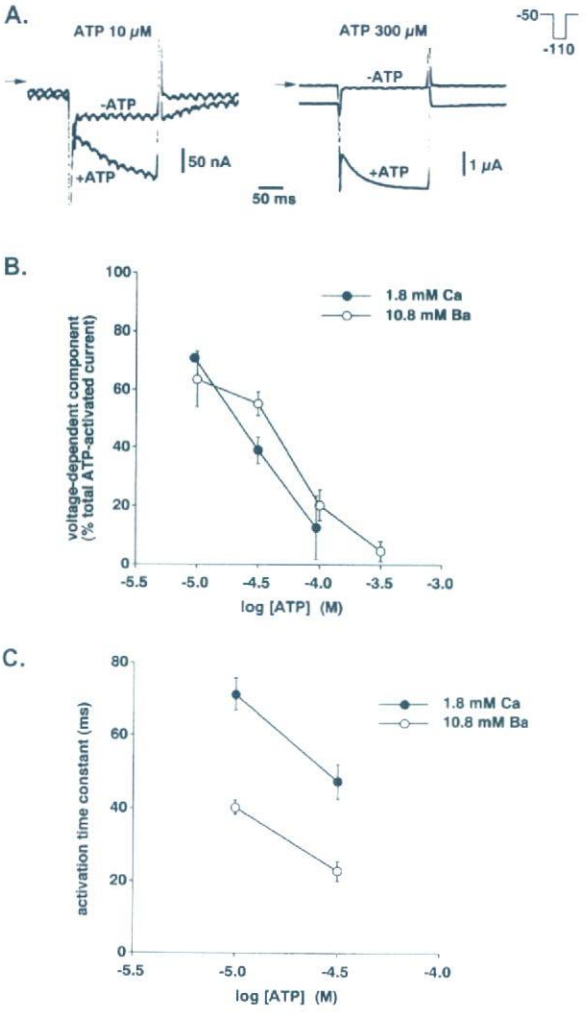

Fig. 3. Effect of ATP concentration. The voltage-dependent current was activated by hyperpolarization (−110 mV) from a holding potential of −50 mV. (A) Voltage-dependent current activated by 10 μM or 30 μM ATP. Current traces in the absence (−ATP) or presence (+ATP) of ATP are superimposed in each panel. (B) Contribution of the voltage-dependent current to total ATP-evoked current using different ATP concentrations. Mean values obtained from 4 oocytes in a standard extracellular solution containing 1.8 mM Ca^{2+} (●) and an extracelllular solution containing 10.8 mM Ba^{2+} (instead of Ca^{2+}; ○) were plotted. Bars represent the S.E.M. (C) Time course of activation of the voltage-dependent components. Time constants were determined as shown in Fig. 1B, and mean values obtained from 4 oocytes were plotted against holding potentials. Bars represent the S.E.M.

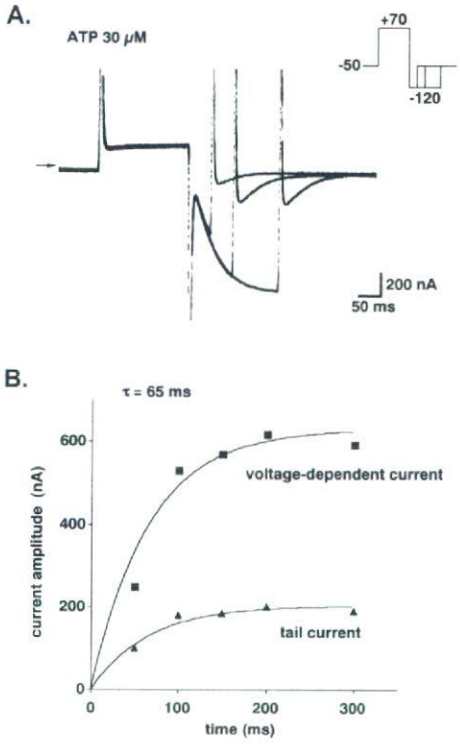

Fig. 4. Activation and tail current. (A) Gradual increase in magnitude of the tail current with increasing voltage-dependent current. Current traces obtained upon exposure to hyperpolarizing pulses (−120 mV) of different durations are superimposed. (B) Time course of activation of the voltage-dependent (■) and tail (▲) currents. Current amplitude was plotted against duration of hyperpolarization (also shown in panel A). The results of both time course activation experiments fit curves with a single time constant of 65 ms.

the relation between activation kinetics of the voltage-dependent component and time course of tail current. As shown in Fig. 4A, oocytes were stepped to 70 mV and then to −120 mV to induce the voltage-dependent component. When hyperpolarization at −120 mV was terminated after various periods, a gradual increase in amplitude of the tail current was observed with increased duration of hyperpolarization at −120 mV. Time courses of both the voltage-dependent component and tail current could be fitted with curves with a single time constant (65 ms in this case; Fig. 4B). Similar fitting with single time constants were made for 4 oocytes tested, and the mean time constant±S.E.M. was 66.3±2.4 ms.

With increased duration of the +70 mV depolarizing pulse, increased amplitude of the voltage-dependent component was observed at −120 mV (Fig. 5A). This may reflect "deactivation" of the voltage-dependent component (Scheme 1):, where A is ATP, and R and R* are closed and open states, respectively, of the voltage-dependent component of $P2X_2$ receptor/channel. The deactivation time course could be fitted with a time constant of 70 ms in this case (Fig. 5B; mean±S.E.M., 71.3±1.3 ms; n=4).

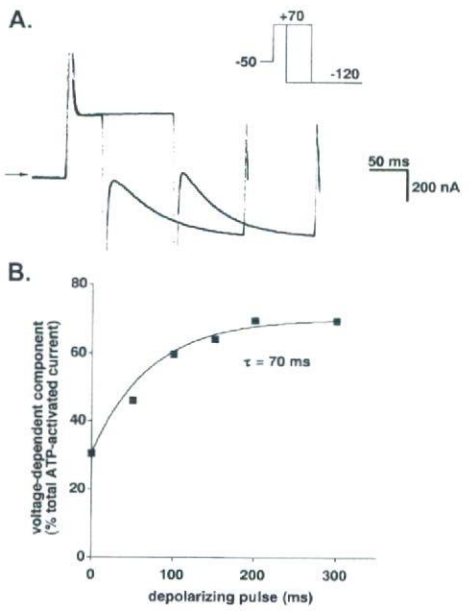

Fig. 5. Deactivation of the voltage-dependent component. (A) Current traces obtained using depolarizing pulses (+70 mV) of two different durations. The amplitude of the voltage-dependent component increased when the duration was prolonged. (B) Time course of deactivation of the voltage-dependent component. Current amplitude was plotted against duration of the depolarizing pulses (also shown in panel A).

3.4. Voltage dependence of activation and deactivation

As shown in Fig. 1, contribution of the voltage-dependent component to total ATP-evoked current was influenced by the holding potential prior to hyperpolarization. This was further examined by testing a number of prepulses at various potentials prior to hyperpolarization (Fig. 6A). As the prepulse became more depolarized, a greater contribution of the voltage-dependent component to total ATP-evoked current was observed, and this contribution became maximal near 0 mV (Fig. 6B). Thus, the voltage-dependent gate must be completely closed at potentials equal to or more positive than 0 mV. The data were fitted with a curve in accordance with the following model of "deactivation":

$$d_\infty = 1/\{1 + \exp[(E_{1/2} - E_m)/k]\}, \quad (1)$$

where d_∞ represents the relative proportion of closed gates at steady state, $E_{1/2}$ is the voltage at which the half-maximal closing occurs, E_m is the membrane potential, and

$$AR \underset{\text{(deactivation)}}{\overset{\text{(activation)}}{\rightleftharpoons}} AR^*$$

Scheme 1.

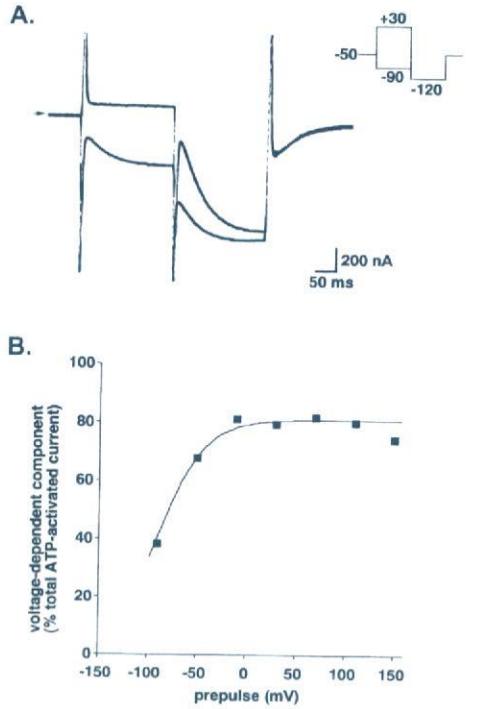

Fig. 6. Prepulse experiment. An ATP concentration of 30 μM was used. (A) Current traces obtained using prepulses of +30 mV ("a") or −90 mV ("b") prior to hyperpolarization at −120 mV. (B) Effect of prepulses. The relative contribution of the voltage-dependent current to total ATP-evoked current at −120 mV was plotted against each prepulse voltage. Some of this data is also shown in panel A.

k is a slope factor reflecting an energy barrier (Hodgkin and Huxley, 1952; Hille, 1992a). As shown in Fig. 6B, potential at which half the gates closed was estimated to be −90 mV in this case (mean±S.E.M., −78.8±5.2 mV; n=4).

The voltage dependence of activation was also examined. As shown in Fig. 7A, the channels responsible for the voltage-dependent component was sufficiently "deactivated" by applying a prepulse of +100 mV, and they were then activated at various hyperpolarization potentials. Contribution of the voltage-dependent component to total ATP-evoked current decreased as the hyperpolarization became more negative up to −45 mV in the case shown in Fig. 7B. Potentials exceeding −45 mV could not be examined since the resultant ATP-evoked current was not large enough to analyze. The data were fitted in accordance with the following model of "activation":

$$a_\infty = 1/\{1 + \exp[(E_{1/2} - E_m)/k]\}, \quad (2)$$

where a_∞ represents the degree of gate opening at steady state. The other parameters are the same as those described above. The data obtained using Eq. (2) (Fig. 7B) could be fitted with a curve indicating that half of the gates were open at a potential of −30 mV.

The above data suggest that activation of the voltage-dependent gate occurs at more positive potentials than gate deactivation. To further investigate this, the fraction of the gates that escaped deactivation ($1-d_\infty$) was calculated from the data obtained during deactivation experiments. The deactivation data was then plotted alongside data obtained from activation experiments (Fig. 7C). These data suggest that the activation potential is 50 mV more positive than the deactivation potential.

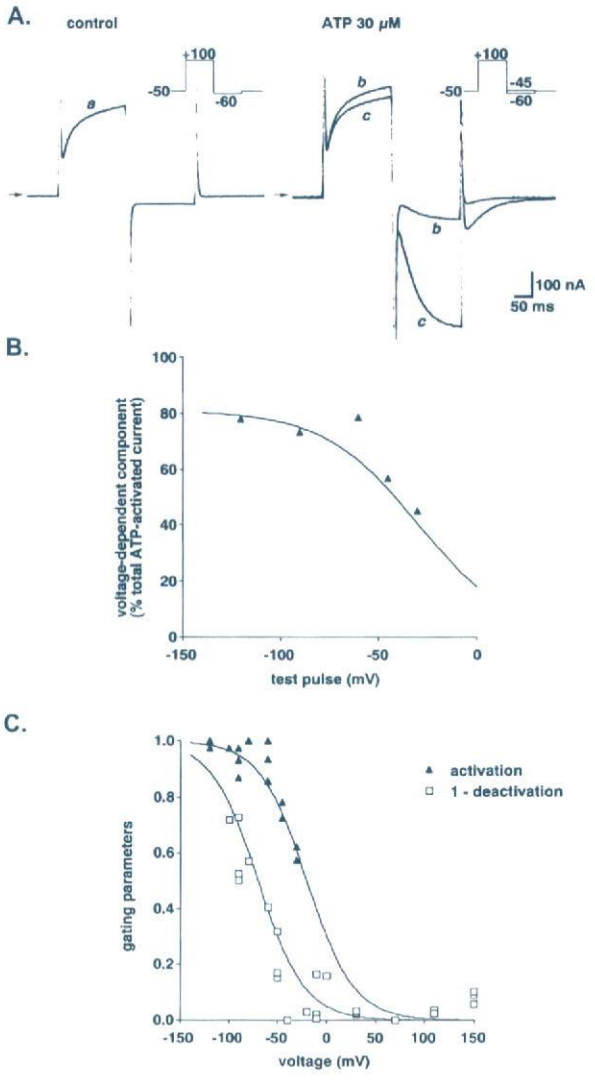

Fig. 7. Effect of hyperpolarization on voltage-dependent current. (A) Current traces before (control) and during the application of 30 μM ATP. In the panel on the right, two current traces obtained following hyperpolarization at −45 mV ("b") and −60 mV ("c") are superimposed. (B) Contribution of voltage-dependent current to total ATP-evoked current at various hyperpolarization potentials. Some of these data are shown in panel A. (C) Comparison of activation and deactivation. Parameters describing activation and deactivation were determined as described in the text. Each data point represents data obtained from individual oocytes.

4. Discussion

4.1. Schematic model of voltage-dependent gating

Recombinant $P2X_2$ receptor/channels expressed in *Xenopus* oocytes exhibited voltage-dependent gating properties similar to those of the channels in PC12 cells (Nakazawa et al., 1997b). The following similarities were observed: (1) the gate opens at negative potentials, (2) activation follows a time course with a time constant of 40 to 70 ms, and (3) gating depends on ATP concentrations. Thus, voltage-dependent gating in PC12 cells may be due to intrinsic expression of $P2X_2$ receptor/channels. We depict here a model that has been proposed to explain voltage-dependent gating of the channels in PC12 cells (Scheme 2):, where A is ATP, R_L and R_H represent closed states, and R* represents the open state (Nakazawa et al., 1997b). In this model, voltage-dependent gating is explained by transition between low and high ATP-affinity states. Upon hyperpolarization, there is a shift from the R_L to the R_H conformation. ATP preferentially binds to channels in the R_H state ($A \cdot R_H$), after which the channels open ($A \cdot R_H^*$). Binding of ATP is the rate-limiting step since activation kinetics were observed to depend on ATP concentrations in the present study (Fig. 3C). The following rate constants have been proposed (Scheme 3): where k_{+1} parallels the concentration of ATP ($k_{+1}=k'_{+1}$[ATP]), and K_d is given by k_{-1}/k'_{+1} (Hille, 1992b). In the present experiment, an activation time constant of 65 ms was observed in the presence of 30 μM of ATP (Fig. 4), which is equivalent to a rate constant of 15 s^{-1}. Using these values, $k'_{+1}=k_{+1}/[ATP]=15\ s^{-1}/(30\ \mu M)=5\times10^5\ M^{-1}\ s^{-1}$. An inactivation time constant of 70 ms was observed in the presence of 30 μM of ATP (Fig. 5), which is equivalent to a rate constant of 14 s^{-1}. Thus, K_d was calculated to be $k_{-1}/k'_{-1}=14\ s^{-1}/(5\times10^5\ M^{-1}\ s^{-1})=28$ μM, which is slightly less than the EC_{50} value obtained at −50 mV (about 40 μM). This estimation is in accordance with the finding that the voltage-dependent component is not completely activated at −50 mV (Fig. 7C). It is difficult to quantify the low-affinity ATP binding state since the relationship between concentration and response needs to be assessed at highly positive potentials, while $P2X_2$ receptor/channels permit only small current due to their inward-rectifying nature. We estimate here the low affinity from simple theoretical concentration–response curves. Fig. 8 shows two concentration–response curves. One demonstrates an EC_{50} of 30 μM, corresponding to a high-affinity state. If the other low-affinity state demonstrates an EC_{50} of 100 μM, more $P2X_2$ receptor/channels were in the high-affinity state in the presence of 10 μM ATP, and more were in the low-affinity state in the presence of 300 μM ATP. This is consistent with the greater observed contribution of the voltage-dependent component to total ATP-evoked current in the presence of 10 μM, while little was observed in the presence of 300 μM ATP (Fig. 3). Thus, the low-affinity state may be lower than the high-affinity state by threefold or larger.

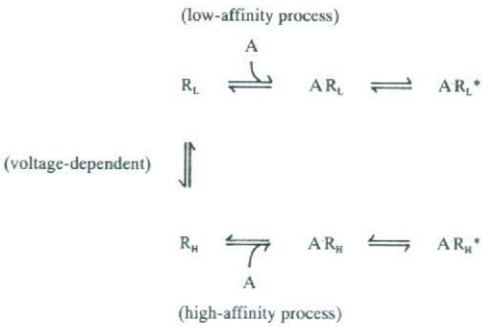

Scheme 2.

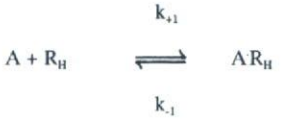

Scheme 3.

The idea of the transition of $P2X_2$ receptor/channels between low- and high-affinity states might explain the "non-voltage-dependent" component of ATP-evoked current. For example, the current evoked by 30 μM ATP was not completely observed as voltage-dependent component even when activated at very negative potentials (Fig. 7B) or following deactivation at very positive potentials (Fig. 6B). This "non-voltage-dependent current" (about 20% of the total ATP-evoked current) might result from the activation of $P2X_2$ receptor/channels in the low-affinity state prior to voltage-dependent activation.

The voltage dependence of activation and deactivation differed, with deactivation occurring at more negative potentials (Fig. 7C). This indicates that the activation and the deactivation do not arise from a simple reversible "back-and-forth" process, rather, two voltage-dependent processes

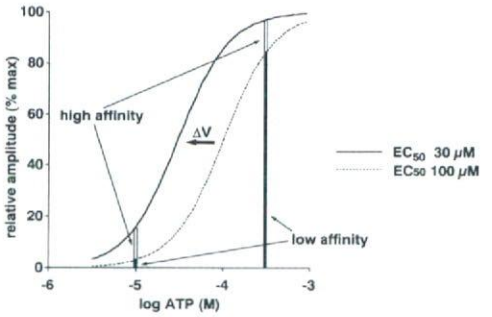

Fig. 8. Voltage-dependent change in sensitivity to ATP might explain dependence of the voltage-dependent current on ATP concentration. Low-affinity (EC_{50}=100 μM) and high-affinity (EC_{50}=30 μM) states of the receptor are thought to exist (Hill coefficient; 1.5). Each receptor shifts from a low-affinity to a high-affinity state upon hyperpolarization (ΔV). With 10 μM ATP, only a small proportion of the receptors, many of which were in the low-affinity state, were activated prior to hyperpolarization, but many more were activated upon induction of the high-affinity state by hyperpolarization. In the presence of 300 μM ATP, a larger proportion of the receptors were activated even in the low-affinity state, and induction of the high-affinity state caused only a marginal increase in activated receptors.

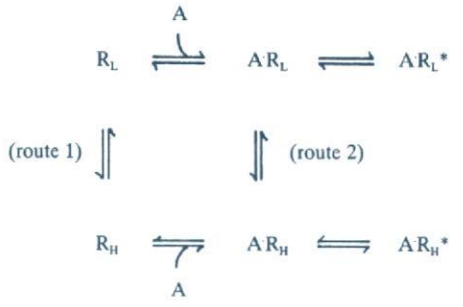

Scheme 4.

may be involved. We propose the following modification to Scheme 2.

This model (Scheme 4) involves two voltage-dependent processes, one resulting in activation through "route 1", and the other resulting in deactivation through "route 2". Such model would explain the observed difference in voltage dependence between activation and deactivation. However, we would expect this model to result in more difficult to interpret data than we did above based on Schemes 2 and 3.

4.2. Relevance of voltage-dependent gating

$P2X_2$ receptor is expressed in a number of neurons (e.g., Atkinson et al., 2000; Rubio and Soto, 2001). $P2X_2$ receptor/channel is permeable to Ca^{2+} (Egan and Khakh, 2004), and Ca^{2+} influx through the channel may influence cellular activity, although its exact role remains to be clarified. The voltage-dependent gating reported here may be relevant to the Ca^{2+} influx from the following consideration. Na^+ current (I_{Na}) and Ca^{2+} current (I_{Ca}) permeating through $P2X_2$ receptor/channel are:

$$I_{Na} = -P_{Na}\frac{E_m F^2}{RT}\frac{[Na]_o}{1-\exp(-EF/RT)} \quad (3)$$

$$I_{Ca} = -4P_{Ca}\frac{E_m F^2}{RT}\frac{[Ca]_o \exp(-2EF/RT)}{1-\exp(-2EF/RT)}, \quad (4)$$

where P_{Na} and P_{Ca} represent the permeability of Na^+ and Ca^{2+}, respectively, E_m represents the membrane potential, and F, R, and T are their usual physicochemical meanings (Fatt and Ginsborg, 1958; Nakazawa et al., 1989). The ratio of I_{Na} to I_{Ca} is thus:

$$\frac{I_{Ca}}{I_{Na}} = \frac{4P_{Ca}[Ca]_o}{P_{Na}[Na]_o}\frac{1}{\exp(E_m F/RT)[\exp(E_m F/RT)+1]} \quad (5)$$

This equation indicates that the ratio of I_{Ca}/I_{Na} is larger at more negative potentials. The ratio calculated at −90 mV is about 13-fold larger than that calculated at −30 mV. Thus, channel opening at negative potentials favors Ca^{2+} over Na^+ influx. Thus, voltage-dependent gating may facilitate cellular Ca^{2+}-dependent responses when cells are hyperpolarized. This may occur when efflux through K^+ channels outpaces depolarization afforded by opening of $P2X_2$ receptor/channels.

4.3. Conclusion

The results of the present study suggested that $P2X_2$ receptor exhibits voltage-dependent gating, and that this is not due to simple activation and deactivation of a single gate, but rather, due to a transition from a low ATP affinity to a high ATP affinity state. This may favor Ca^{2+} influx at negative potentials, although further studies are required to clarify the physiological significance of voltage-dependent gating of $P2X_2$ receptor.

Acknowledgements

This work was supported, in part, by a Health and Labour Science Research Grant for Research on Advanced Medical Technology from the Ministry of Health, Labour and Welfare, Japan, as well as a grant-in-aid for scientific research from the Ministry of Education, Science, Sports and Culture, Japan (KAKENHI 13672319) awarded to K.N.

References

Atkinson, L., Batten, T.F., Deuchars, J., 2000. $P2X_2$ receptor immunoreactivity in the dorsal vagal complex and area postrema of the rat. Neuroscience 99, 683–696.

Brake, A.J., Wagenbach, M.J., Julius, D., 1994. New structural motif for ligand-gated ion channels defined by an ionotropic ATP receptor. Nature 371, 519–523.

Clyne, J.D., LaPointe, L.D., Hume, R.I., 2002. The role of histidine residues in modulation of the rat $P2X_2$ purinoceptor by zinc and pH. J. Physiol. 539, 347–359.

Egan, T., Khakh, B.S., 2004. Contribution of calcium ions to P2X channel responses. J. Neurosci. 24, 3413–3420.

Egan, T.M., Haines, W.R., Voigt, M.M., 1998. A domain contributing to the ion channel of ATP-gated $P2X_2$ receptors identified by the substituted cysteine accessibility method. J. Neurosci. 18, 2350–2359.

Ennion, S., Hagan, S., Evans, R.J., 2000. The role of positively charged amino acids in ATP recognition by human $P2X_1$ receptors. J. Biol. Chem. 275, 29361–29367.

Fatt, P., Ginsborg, B.L., 1958. The ionic requirements for the production of action potentials in crustacean muscle fibres. J. Physiol. 142, 516–543.

Haines, W.R., Migita, K., Cox, J.A., Egan, T.M., Voigt, M.M., 2001. The first transmembrane domain of the P2X receptor subunit participates in the agonist-induced gating of the channel. J. Biol. Chem. 276, 32793–32798.

Hille, B., 1992a. Classical biophysics of the squid giant axon. Ionic channels of excitable membranes, Second Edition. Sinauer, Sunderland, MA, pp. 23–58.

Hille, B., 1992b. Ligand-gated channels of fast chemical synapses. Ionic channels of excitable membranes, Second Edition. Sinauer, Sunderland, MA, pp. 140–169.

Hodgkin, A.L., Huxley, A.F., 1952. The dual effect of membrane potential on sodium conductance in the giant axon of *Loligo*. J. Physiol. 116, 497–506.

Jiang, L.H., Rassendren, F., Surprenant, A., North, R.A., 2000. Identification of amino acid residues contributing to the ATP-binding site of a purinergic P2X receptor. J. Biol. Chem. 275, 34190–34196.

Jiang, L.H., Rassendren, F., Spelta, V., Surprenant, A., North, R.A., 2001. Amino acid residues involved in gating identified in the first membrane-spanning domain of the rat $P2X_2$ receptor. J. Biol. Chem. 276, 14902–14908.

Khakh, B.S., 2001. Molecular physiology of P2X receptors and ATP signalling at synapses. Nat. Rev. 2, 165–174.

Migita, K., Haines, W.R., Voigt, M.M., Egan, T.M., 2001. Polar residues of the second transmembrane domain influence cation permeability of the ATP-gated $P2X_2$ receptor. J. Biol. Chem. 276, 30934–30941.

Nakazawa, K., Ohno, Y., 1997. Effects of neuroamines and divalent cations on cloned and mutated ATP-gated channels. Eur. J. Pharmacol. 325, 101–108.

Nakazawa, K., Fujimori, K., Takanaka, A., Inoue, K., 1989. An ATP-activated conductance in pheochromocytoma cells and its suppression by extracellular calcium. J. Physiol. 428, 257–272.

Nakazawa, K., Liu, M., Inoue, K., Ohno, Y., 1997a. pH dependence of facilitation by neurotransmitters and divalent cations of $P2X_2$ purinoceptor/channels. Eur. J. Pharmacol. 337, 309–314.

Nakazawa, K., Liu, M., Inoue, K., Ohno, Y., 1997b. Voltage-dependent gating of ATP-activated channels in PC12 cells. J. Neurophysiol. 78, 884–890.

Nakazawa, K., Ojima, H., Ohno, Y., 2002. A highly conserved tryptophane residue indispensable for cloned rat neuronal P2X receptor activation. Neurosci. Lett. 324, 141–144.

North, R.A., 2002. Molecular physiology of P2X receptors. Physiol. Rev. 82, 1013–1067.

North, R.A., Surprenant, A., 2000. Pharmacology of cloned P2X receptors. Annu. Rev. Pharmacol. Toxicol. 40, 563–580.

Ralevic, V., Burnstock, G., 1998. Receptors for purines and pyrimidines. Pharmacol. Rev. 50, 413–492.

Rassendren, F., Buell, G., Newbolt, A., North, R.A., Surprenant, A., 1997. Identification of amino acid residues contributing to the pore of a P2X receptor. EMBO J. 16, 3446–3454.

Roberts, J.A., Evans, R.J., 2004. ATP binding at human $P2X_1$ receptors. Contribution of aromatic and basic amino acids revealed using mutagenesis and partial agonists. J. Biol. Chem. 279, 9043–9055.

Rubio, M., Soto, F., 2001. Distinct localization of P2X receptors at excitatory postsynaptic specializations. J. Neurosci. 21, 641–653.

Weber, W.-M., 1999. Ion currents of *Xenopus laevis* oocytes: state of the art. Biochim. Biophys. Acta 1421, 213–233.

Zhang, Y., Hamill, O.P., 2000. Calcium, voltage- and osmotic stress sensitive currents in *Xenopus* oocytes and their relationship to single mechanically gated channels. J. Physiol. 523, 83–99.

Available online at www.sciencedirect.com

SCIENCE DIRECT

European Journal of Pharmacology 518 (2005) 107 – 110

www.elsevier.com/locate/ejphar

Short communication

Purification and aqueous phase atomic force microscopic observation of recombinant $P2X_2$ receptor

Ken Nakazawa [a,*], Yoko Yamakoshi [b,1], Toshie Tsuchiya [c], Yasuo Ohno [a]

[a] *Division of Pharmacology, National Institute of Health Sciences, 1-18-1 Kamiyoga, Setagaya, Tokyo 158-8501, Japan*
[b] *Division of Organic Chemistry, National Institute of Health Sciences, 1-18-1 Kamiyoga, Setagaya, Tokyo 158-8501, Japan*
[c] *Division of Medical Devices, National Institute of Health Sciences, 1-18-1 Kamiyoga, Setagaya, Tokyo 158-8501, Japan*

Received 4 April 2005; received in revised form 14 June 2005; accepted 20 June 2005
Available online 28 July 2005

Abstract

Recombinant $P2X_2$ receptor was observed by atomic force microscope in the aqueous phase. The $P2X_2$ receptor was expressed in an insect cell line, and recombinant proteins were prepared under native conditions. The membrane fractions were extracted, and histidine-tagged receptor protein was purified from the fractions by column chromatography. When the purified protein fraction was diluted with water and served for atomic force microscopy, dispersed particles of about 3 nm in height were observed. In the presence of 1 mM ATP, the assembly-like images of the particles were obtained. More densely assembled images of the particles were achieved when the protein was dissolved in a Tris buffer containing 1 mM ATP. Under this condition, imaging of the surface of the particles exhibited a circular structure with a diameter of about 10 nm having a pore-like structure. These results suggest that atomic force microscopy provides structural information about $P2X_2$ receptor in aqueous phase.

Keywords: P2X receptor; Atomic force microscopy; Protein structure; ATP

1. Introduction

P2X receptors are ion channel forming membrane proteins that are activated by extracellular ATP, and their physiological roles have been shown in various tissues including the central nervous system (see reviews, Khakh, 2001; North, 2002; Vial et al., 2004). This ion channel/receptor family consists of 7 subclasses ($P2X_1$ to $P2X_7$), and is believed to have molecular structures distinct from so-called "ligand-gated channel super family" including nicotinic acetylcholine receptor/channels and ionotropic glutamate receptor channels. Structural analyses such as the X-ray crystal analysis have not been made for P2X receptor/channel family. In addition, because of their distinct structures, estimation from homology modeling based on known three-dimensional structures of other proteins is difficult. Thus, information concerning the structure and morphology of P2X receptor is lacking. Atomic force microscopy is an approach for structural analysis that allows the analysis of a small amount (nanogram to microgram) of uncrystalized protein. Atomic microscopy enables the observation of both individual and assembled protein molecules in the aqueous phase, which may reveal dynamic forms of biologically active proteins (Müller and Engel, 2002). Recently, Barrera et al. (2005) reported atomic force microscopy imaging of dried P2X receptor protein. In the present study, we have prepared $P2X_2$ receptor protein from an insect cell line expression system, and made atomic force microscopy imaging in aqueous phase. The imaging has revealed that $P2X_2$ receptor is a pore-forming protein for the first time.

* Corresponding author. Tel.: +81 3 3700 9704; fax: +81 3 3707 6950.
E-mail address: nakazawa@nihs.go.jp (K. Nakazawa).
[1] Present address: Center for Polymers and Organic Solids, Department of Chemistry and Biochemistry, University of California, Santa Barbara, CA 93106-9510, USA.

0014-2999/$ - see front matter © 2005 Elsevier B.V. All rights reserved.
doi:10.1016/j.ejphar.2005.06.018